Development of reduction-responsive degradable polylactide-based amphiphilic block copolymers for drug-delivery applications.

Alexander J. Cunningham

A Thesis
in
the Department
of
Chemistry and Biochemistry

Presented in Partial Fulfillment of the Requirements
for the Degree of Master of Science (Chemistry) at
Concordia University
Montréal, Quebec, Canada

August 2014

© Alexander J. Cunningham, 2014

CONCORDIA UNIVERSITY

School of Graduate Studies

This is to certify that the thesis prepared

By: **Alexander J. Cunningham**

Entitled: Development of stimuli-responsive degradable polylactide-based amphiphilic block copolymers for drug-delivery applications.

and submitted in partial fulfillment of the requirements for the degree of

Master of Science (Chemistry)

complies with the regulations of the University and meets the accepted standards with respect to originality and quality.

Signed by the final examining committee:

_____ Chair

_____ Examiner
Dr. Pat Forgione

_____ Examiner
Dr. Xavier Ottenwaelder

_____ Supervisor
Dr. John Oh

Approved by _____
Chair of Department or Graduate Program Director

_____
Dean of Faculty

Development of reduction-responsive degradable polylactide-based amphiphilic block copolymers for drug-delivery applications.

Alexander J. Cunningham

Ubiquitous in nature as a result of their versatility both in their structure and properties, smart polymers have been the subject of intensive research in the design of synthetic materials in the field of biomedicine. Of notable consideration, these polymers as drug delivery vehicles offer the potential to increase the bioavailability of therapeutic molecules while reducing the side effects customarily associated with small molecule delivery.

Amphiphilic block copolymers (ABPs) bear a hydrophobic block comprising the hydrophobic core of the nanostructure, and a hydrophilic block providing colloidal stability. The ABP-based micellar carriers are endowed with great advantages that include, but are not limited to, the use of biocompatible material in their synthesis, thereby avoiding adverse side effects from the use of noxious materials. Moreover, the material can be synthesized using facile synthetic methods that allow a narrow size distribution and versatility in their physicochemical properties. Furthermore, their chemical flexibility in their design allows for the incorporation of targeting ligands at the hydrophilic corona promoting active targeting into specific cells. Another point to consider is the incorporation of dynamic chemical bonds in the architecture of the delivery vehicle to promote spatio-temporal release of the encapsulated cargo. Known as stimuli-responsive degradation (SRD), this concept has been exercised to take advantage of endogenous cellular triggers such as gradients in redox potential, pH or temperature that exists among different sub-cellular organelles as well as in

different cell types/states; e.g. healthy vs. cancerous cells. One such promising stimuli-responsive platform is the disulfide-thiol chemistry.

In addition, polylactide, a hydroxyalkanoic acid-based hydrophobic polyester, is a promising material in the synthesis of ABPs for biomedical applications. Indeed, it is biocompatible, biodegradable, FDA-approved, and has tunable mechanical properties. However, two challenges remain to be resolved before a successful polylactide-based drug delivery system can be developed: 1) its inherent hydrophobicity; 2) its slow degradation. In this thesis, potential solutions are examined.

This research is based on the development of monocleavable thiol-responsive degradable polylactide-based amphiphilic block copolymers for drug delivery applications. Different synthetic strategies for the preparation of disulfide-labeled ABPs are presented using either a methacrylate-based or an ethylene oxide-based hydrophilic block. These ABPs are synthesized by a combination of ring-opening polymerization with either atom-transfer radical polymerization or a facile coupling reaction. They are amphiphilic and thus self-assemble to form colloidaly stable micellar aggregates in aqueous solutions above their critical micellar concentration (CMC). These drug loaded ABPs were tested for drug delivery by studying the extent of drug loading and release through analytical methods. Results suggest the disulfide-labeled ABPs respond to the presence of a reducing agent by releasing the encapsulated drug providing support for their potential as delivery vehicles for the targeted release of loaded drugs in both time and space.

Acknowledgements

I would like to thank my supervisor Dr. John Oh for his support, his mentorship, and his guidance. He has helped in tremendous ways into shaping me into a great scientist. He has been a true mentor for me, helping me develop and attain my goals, always present and accessible, always prompt to teach and instruct, yet friendly and welcoming. Undoubtedly, working for him has been a great pleasure, and yet a great training.

Also, I would like to thank my committee members Drs. Xavier Ottenwaelder and Pat Forgione for their advice and helpful discussions. They have been there for me whether I had a question or concern and for that I am very grateful. In addition, their questions and insight into my research has helped me progress enormously.

Additionally, I would like to thank Drs. Judith and Jack Kornblatt. Their doors always open, they have guided me and advised me in countless ways. Their kindness and support has made my stay at Concordia pleasant and delightful. Moreover, they have been a mentor for me and have greatly contributed into helping me achieve my goals.

Moreover, I would like to thank my colleagues for their helpful discussions in the lab and the wonderful time we spent.

J`aimerais remercier ma mère et mon père pour leur présence dans ma vie et leur support. Là pour moi pendant toutes ces années, patients et supportant, aimant et chaleureux, je ne pourrai jamais oublier tout ce qu`ils ont fait pour moi. Leur présence dans ma vie a été une source de joie et de réconfort. Ils ont été instrumental à devenir qui je suis et pour ça je leur serai toujours reconnaissant.

J`aimerais remercier la famille Robinson, Mattieu, Stéphane, Emmanuel Mr. et Mme. Robinson, pour tout ce qu`ils ont fait pour moi. Leur aide et support est indescriptible. De toutes les bénédictions que Dieu m`a donné les avoir dans ma vie est de loin la plus belle et celle dont je chéri le plus. Ils sont pour moi un havre de paix, une source de joie, un réconfort dans les temps difficile et un partenaire dans les temps de joie. Leur sagesse et intelligence sont contagieuses, toujours prompt à aider et encourager, ils ont été instrumentaux dans mon développement personnel et dans ma marche vers Dieu. J`aimerais particulièrement souligner l`aide et le support de Mattieu et Stéphane pendant la rédaction de cette thèse; ils m`ont épaulé, encouragé, fortifié, mais surtout ils m`ont démontré un amour et une complicité que seuls des frères auraient pu démontrer. J`aimerais aussi les remercier pour tous ce qu`ils ont fait pour moi et tous les merveilleux moments que nous avons passé ensemble. Dans mes moments difficiles ils ont été la et m`ont aidé à me relever et je ne pourrai jamais les remercier assez. J`aimerais également remercier Mr. et Mme Robinson pour toutes leurs prières et leur conseils, et tous ces bons moments que nous avons passé ensemble, ils m`ont traité comme leur fils et ont été comme des parents pour moi, et je ne pourrai jamais oublier tout ce qu`ils ont fait. Finalement, j`aimerais remercier Emmanuel pour tous ses conseils et tous ces merveilleux moments passé ensemble, lui aussi présent dans les moments difficiles il a été là pour moi et je lui suis reconnaissant pour tout. Ce que je suis devenu est en grande partie grâce à eux et pour ceci, je les remercie.

J`aimerais aussi prendre ce moment pour remercier Alexandru Ionescu et Tamara Dupuy pour leur aide et leur support.

Finalement, j`aimerais remercier Dieu qui m`a donné la vie, la joie, l’espérance, la rédemption. Il m`a béni de sa grâce et de sa miséricorde. Il est ma source d`amour et de joie, le soleil dans ma vie, mon rempart et mon bouclier, le

rocher de mon salut, mon espérance et mon allégresse, mon saint-berger et mon maitre, mon père et mon créateur. Il me soutient de sa droite triomphante, et par sa grâce ma rendu vainqueur. J`aimerais remercier Jésus-Christ, mon seigneur et sauveur, pour la rédemption de mes péchés et pour son amour éternel; dans ma détresse Il me porta secours, me sorti des ténèbres et de l`ombre de la mort, me délivra de mes angoisses, arracha mes liens, et me fit voir la lumière, Sa lumière. YHWH, Éternel très-Haut, en toi je mets mon espérance et je désire te servir pour l`éternité, que Ton nom soit béni, et Ton règne vienne, que Ta volonté soit faite sur la terre comme elle est faite dans les cieux.

Contribution of Authors

The majority of the research conducted in the presented thesis was conducted independently under the supervision of Dr. John Oh at Concordia University. The chapters 3 and 4 are reproduced in part, with approval from the publisher, from the original article from which they are drawn.

Chapter 3 was reproduced from *Macromolecular Rapid Communications* **2013**, *34*, 163-168. While I am the primary author and I conducted the bulk of the research, Behnoush Khorsand conducted the cell viability experiments, although the data is not presented here.

Chapter 4 was reproduced from *Colloids and Surfaces B: Biointerfaces*, **2014,** *In press, DOI: 10.1016/j.colsurfb.2014.08.002*. While I am the primary author and I conducted the bulk of the research, Na Re Ko, a contributor to this manuscript, conducted the cell viability experiments, although the data is not presented here.

Table of Contents

List of Figures xii

List of Abbreviations xv

Chapter 1 Introduction 1

1.1 Overview of research and goals 1

1.2 Drug delivery general understanding and goals 1

1.3 Polymer-based drug delivery applications 2

1.3.3 ABP-based drug delivery nanocarriers 5

1.3.4 Micellization of ABP 6

1.3.4.1 Micelle size 8

1.3.5 Micelle preparation 9

1.4 Stimuli-responsive copolymers in drug delivery 11

1.4.1 Stimuli-responsive covalent linkages 12

1.4.2 Approaches to preparation of reduction-responsive micelles at different locations 13

1.5 Biocompatible polylactide and their nanomaterials 15

1.5.1 Polylactide and its challenges in biomedical applications 15

1.5.2 Literature related monocleavable micelles 17

1.6 Scope of the thesis 19

Chapter 2 21

Methodology: Synthesis and Characterization 21

2.1. Brief description 21

2.2 Synthesis and characterization of triblock copolymers 21

2.2.1 ROP for the synthesis of PLA 21

2.2.1 ATRP for the synthesis of ABP 24

2.2.2 Copolymer characterization: Gel permeation chromatography (GPC) 26

2.3 Aqueous micellization and characterization 28

2.3.1 Preparation of micellar aggregates 28
2.3.2 Determination of critical micellar concentration (CMC) 28
2.3.3 Size and morphology characterization 30
Chapter 3 32
New design of thiol-responsive PLA-based triblock copolymer micelles 32
3.1 Introduction 34
3.2 Experimental 36
3.2.1 Instrumentation and analyses 36
3.2.2 Thermal analysis 37
3.2.3 Materials 37
3.2.4 Synthesis of ss(PLA-OH)$_2$ by ROP 37
3.2.5 Esterification to ss(PLA-Br)$_2$ 38
3.2.6 Synthesis of ssABP-1 by ATRP 38
3.2.7 Aqueous micellization 39
3.2.8 Determination of critical micellar concentration (CMC) using a NR probe 39
3.2.9 Reductive degradation of ss(PLA-OH)$_2$ and ssABP-1 in DMF 40
3.2.10 Thiol-responsive degradation of aqueous micelles 41
3.2.11 Encapsulation of Dox 41
3.2.12 Release of Dox from Dox-loaded micelles upon thiol-responsive degradation 41
3.3 Results and discussion 42
3.3.1 Synthesis of ssABP-1 from a combination of ROP and ATRP 42
3.3.2 Aqueous micellization of ssABP-1 45
3.3.3 Reduction-responsive disulfide bond cleavage 46
3.3.4 Thiol-triggered drug release from Dox-loaded ssABP-1 50
3.4 Conclusion 51
Chapter 4 52
Alternative method to synthesize reduction-responsive PLA-based monocleavable micelles 52

4.1 Introduction 54
4.2 Experimental 56
4.2.1 Instrumentation and analyses 56
4.2.2 Transmission Electron Microscope (TEM) images 56
4.2.3 Materials 56
4.2.4 Synthesis of ss(PLA-OH)$_2$ by ROP 56
4.2.5 Carboxylation of ss(PLA-OH)$_2$ to ss(PLA-COOH)$_2$ 57
4.2.6 Synthesis of ssABP-2 by DCC coupling 57
4.2.7 Determination of critical micellar concentration (CMC) using a NR probe 58
4.2.8 Aqueous self-assembly 58
4.2.9 Reductive cleavage of disulfide linkages in ssABP-2 58
4.2.10 Reduction-responsive degradation of ssABP-2 micelles 58
4.2.11 Encapsulation of Dox 59
4.2.12 GSH-triggered Dox release from Dox-loaded micelles 59
4.2.13 Non-specific interaction of ssABP-2 micelles with BSA 59
4.3 Results and discussion 61
4.3.1 Synthesis of ssABP-2 61
4.3.2 Aqueous micellization of ssABP-2 64
4.3.3 Thiol-induced degradation of ssABP-2 triblock copolymers 66
4.3.4 Loading and thiol-triggered drug release from Dox-loaded ssABP 69
4.3.5 Non-specific protein interaction of ssABP-2 in vitro 71
4.4 Conclusion 72
Chapter 5 74
Conclusion and future work 74
References 78
Appendix A 84
Appendix B 87
Publications 89

List of Figures

Figure 1.1. Different types of polymer-based DDS. 3
Figure 1.2. An illustration of self-assembly of ABPs into different aggregates. 6
Figure 1.3. Drug accumulation into cancer tissues arising from the enhanced permeation and retention effect (EPR). 9
Figure 1.4. Stimuli-responsive degradation for the spatio-temporal release of encapsulated therapeutic drugs in the nanoparticles 12
Figure 1.5. Different positions and numbers for the location of SRD groups in the architecture of the polymer enabling spatio-temporal drug release. 15
Figure 1.6. D,L-polylactide. 16
Figure 2.1. Scheme for the (a) anionic ROP of LA and (b) cationic ROP of LA in the presence of methyl trifluoromethanesulfonate (MeOTf). 22
Figure 2.2. Mechanism for the coordination-insertion ROP for the synthesis of PLA in the presence of Sn(II) 2-ethylhexanoate 24
Figure 2.3. Mechanism for ATRP polymerization. 26
Figure 2.4. Principle for separation of polymers according to hydrodynamic volume 27
Figure 2.5. Twisted intramolecular chain transfer leading to NR excited state. 30
Figure 3.1. Synthetic strategy for the preparation of PLA-based monocleavable triblock copolymers. 42
Figure 3.2. 1H-NMR spectra of ss(PLA-OH)2, ss(PLA-Br)2, ssABP-1 in CDCl3 where x denotes a trace of THF (a), GPC traces of ssABP-1 compared with ss(PLA-OH)2 precursor (b). 45
Figure 3.3. Fluorescence intensity of Nile Red for aqueous mixtures consisting of NR with various amounts of ssABP-1 to determine the CMC (a), DLS diagram of ssABP-1 micelles at a concentration of 0.1 mg/mL in deionized water (b). 46

Figure 3.4. GPC results for the degradation of ss(PLA-OH)2 (a) and ssABP-1 (b) mixed with 5 mole equivalent DTT to disulfides in DMF..... 48
Figure 3.5. DLS diagram of ssABP-1-based micelles before (a) and 2 days after (b) the addition of DTT and GPC traces of ssABP-1 micelles without and with 10 mM DTT after removal of water (c). 49
Figure 3.6. % release profiles of Dox from Dox-loaded micelles in the absence (control) and presence of 10 mM GSH in PBS solution adjusted at pH = 7.4. 51
Figure 4.1. Synthetic strategy for the preparation of well-controlled reduction-responsive ssABP-2 triblock copolymers. 55
Figure 4.2. GPC traces of ssABP-2, compared with ss(PLA-OH)2 and PEO precursors. 62
Figure 4.3. ^{1}H-NMR spectra of purified ss(PLA-OH)2 (a) and ss(PLA-COOH)2 (b) in $CDCl_3$. 62
Figure 4.4. ^{1}H-NMR spectrum of ssABP-2 in $CDCl_3$. 64
Figure 4.5. Overlaid fluorescence spectra (inset) and fluorescence intensity at λ = 620 nm for aqueous mixtures consisting of NR with various amounts of ssABP-2 to determine the CMC..... 65
Figure 4.6. DLS diagrams (a, c) and TEM images (b, d) of aqueous micelles before (a, b) and after (c, d) treatment with 10mM DTT in aqueous solution at 1.3 mg/mL. 66
Figure 4.7. GPC traces of ssABP-2 before and after treatment with DTT in DMF as well as ssABP-2 micelles treated with DTT and GSH in water. For micelle sample, water was removed for GPC measurements. 68
Figure 4.8. DLS diagram of aqueous ssABP-2-based micelles in the presence of 10 mM DTT (a) and 10 mM GSH (b) over time. 69
Figure 4.9. % Release profiles of Dox from Dox-loaded micelles in the absence (control) and presence of 10 mM GSH in PBS solution adjusted at pH = 7.4. 71

Figure 4.10. DLS diagrams of mixture consisting of ssABP-2 micelles and BSA at weight ratio of micelle/BSA = 1/1 (13 mg/mL) and 1/2 (26 mg/mL) in PBS solution at pH = 7.4 after 90 hrs. 72
Figure A.1. Figure A.1. First-order kinetic plot (a) and evolution of molecular weight and molecular weight distribution over conversion (b) for ATRP of OEOMA in the presence of ss(PLA-Br)2 macroinitiator in THF at 47 °C. Conditions: [OEOMA]0/[ss(PLA-Br)2]0/[CuBr/PMDETA]0 = 20/1/0.5; OEOMA/THF = 0.8/1 wt/wt. The dotted lines are linear fits and the line in (b) is the theoretically predicted molecular weight over conversion. 84
Figure A.2. ^{1}H-NMR spectra, in CDCl3, of ss(PLA-OH)2 (a) and DTT-mediated degraded product (HS-PLA-OH) (b) yielded by the cleavage of disulfides. X denotes a residure of THF. 85
Figure A.3. UV/Vis spectrum of Dox-loaded micelles in a mixture of DMF/water = 5/1 v/v. 85
Figure A.4. Evolution of fluorescence spectra of outer water in the absence (a) and presence (b) of 10 mM GSH along with fluorescence spectra used for normalization as a mimic of 100% drug release. 86
Figure B.1. GPC traces of ss(PLA-COOH)2 (a), and PEO (b), and crude ssABP-2 before purification (c). 87
Figure B.2. UV/Vis spectrum of Dox-loaded micelles in a mixture of DMF/water = 5/1 v/v.. 88
Figure B.3. Evolution of fluorescence spectra of outer water in the absence (a) and presence (b) of 10 mM GSH along with fluorescence spectra used for normalization as a mimic of 100% drug release. 88

List of Abbreviations

ABP	Amphiphilic block copolymer
BSA	Bovine serum albumin
Br-iBuBr	α-Bromoisobutyryl bromide
$CDCl_3$	d-Chloroform
CMC	Critical micellar concentration
CuBr	Copper(I) bromide
DCC	*N,N′*-dicyclohexylcarbodiimide
DCU	Dicyclohexylurea
DCM	Dichloromethane
DDS	Drug delivery system
DLS	Dynamic light scattering
DMAP	4-(dimethylamino)pyridine
DMF	*N,N*-Dimethylformamide
Dox	Doxorubicin
DTT	DL-dithiothreitol
EPR	Enhanced permeability and retention effect
Et_3N	Triethylamine
FL	Fluorescence
GPC	Gel permeation chromatography
GSH	Glutathione
HEMI	*N*-(2-hydroxyethyl) maleimide
KH_2PO_4	Monopotassium phosphate
LA	Lactide
MeOH	Methanol
M_n	Number-average molecular weight
M_w	Weight-average molecular weight
MWCO	Molecular weight cut-off
NMR	Nuclear magnetic resonance
NP	Nanoparticle
NR	Nile Red
OEOMA	Oligo(ethylene glycol) monomethyl ether methacrylate
PCL	Polycaprolactone
PDI	Polydispersity
PEO	Poly(ethylene oxide)

PLA	Polylactide
PMDETA	*N,N,N′,N″,N″*-Pentamethyldiethylenetriamine
PMMA	Poly(methyl methacrylate)
PSt	Polystyrene
RAFT	Reversible addition-fragmentation chain transfer
RES	Reticulo-endothelial system
RI	Refractive index
ROP	Ring-opening polymerization
SA	Succinic anhydride
$Sn(Oct)_2$	Tin(II) 2-ethylhexanoate
SRD	Stimuli-responsive degradation
SS	Disulfide
ssDOH	2-hydroxyethyl disulfide
TEM	Transmission electron microscope
T_g	Glass-transition temperature
THF	Tetrahydrofuran
UV/Vis	Ultraviolet/Visible

Chapter 1 Introduction

1.1 Overview of research and goals

The goal of my master`s research is to explore novel methods for the synthesis of disulfide-labeled amphiphilic block copolymers (ABP) that can be useful as effective building blocks to fabricate drug delivery vehicles exhibiting controlled/enhanced release of anti-cancer drugs in specific tissues. Specifically, two polylactide (PLA)-based monocleavable amphiphilic triblock copolymers with a disulfide linkage in the middle of the hydrophobic block were designed to study the impact of architectural morphology on reduction-responsive degradation and concomitant drug release. These monocleavable PLA-based ABPs were synthesized by ring-opening polymerization (ROP) combined with either atom-transfer radical polymerization (ATRP) or a facile coupling reaction. They self-assembled into micellar aggregates having disulfides in their hydrophobic core, allowing the encapsulation of hydrophobic drugs, and surrounded with hydrophilic coronas, ensuring colloidal stability. The reductive cleavage of the disulfide linkages resulted in a change in the morphology of micellar aggregates as well as an enhanced release of encapsulated anti-cancer drugs.

1.2 Drug delivery general understanding and goals

In the treatment of various diseases, small therapeutics are chemically synthesized to remedy the function of diseased enzyme or state. Almost 60 years ago Sidney Farber successfully conducted the first clinical trial for a chemotherapeutic agent against a tumor.[1] Unfortunately, these small therapeutics displayed various side effects and limitations. One commonly associated side effect encountered in chemotherapy is the nonspecific toxicity.[2] On one hand,

these molecules often target general cellular pathways common to every cell in the organism; on the other hand these molecules are small enough to pass through endothelial cells and gain access to various tissues thereby causing toxic responses in healthy tissues. A promising solution is to construct effective drug delivery systems that can prevent the nonspecific toxicity associated with traditional small molecule therapies.[2-3]

1.3 Polymer-based drug delivery applications

1.3.1 Characteristics of polymer-based drug delivery

In order to circumvent the toxicity associated with small molecule therapy, drug delivery vehicles has been proposed as a means to encapsulate these drug molecules and deliver them safely and efficiently to the targeted tissue. Building on the idea of the magic bullet, proposed by Paul Erlich, numerous devices have been designed to incorporate hydrophobic drugs effectively shielding it during transportation throughout the blood stream.[4] Typical examples of such strategies include inorganic-based nanoparticles,[5] polypeptide-drug conjugates,[6] polymer-drug conjugates,[7] and polymer based nanoparticles.[8] Particularly, polymer-based nanoparticles have displayed superior advantages in some regards; notably in the sense that they can be prepared from biocompatible materials that limits issues of compliance between the synthetic material and the physiological milieu; have a wide range of structures that can be obtained; and have tunable chemical and physical properties.[9] The advantages that delivery systems can confer to the small therapeutics include 1) protection of therapeutics during blood circulation thereby avoiding possible deactivation through enzymatic reactions or other interactions; 2) enhanced uptake into targeted cells through incorporation of targeting ligands for receptor-mediated endocytosis; 3) avoidance of renal

clearance; 4) increased biodistribution and circulation time thereby increasing the likelihood of the drug to reach the targeted tissue.

1.3.2 Shapes and structures of polymer-based drug delivery systems

Figure 1.1 shows different types of polymer-based drug delivery systems (DDS) that have been developed; they include polymer-drug conjugates,[7b, 10] dendrimers,[11] microgels/nanogels,[12] and block copolymer aggregates.[8, 13]

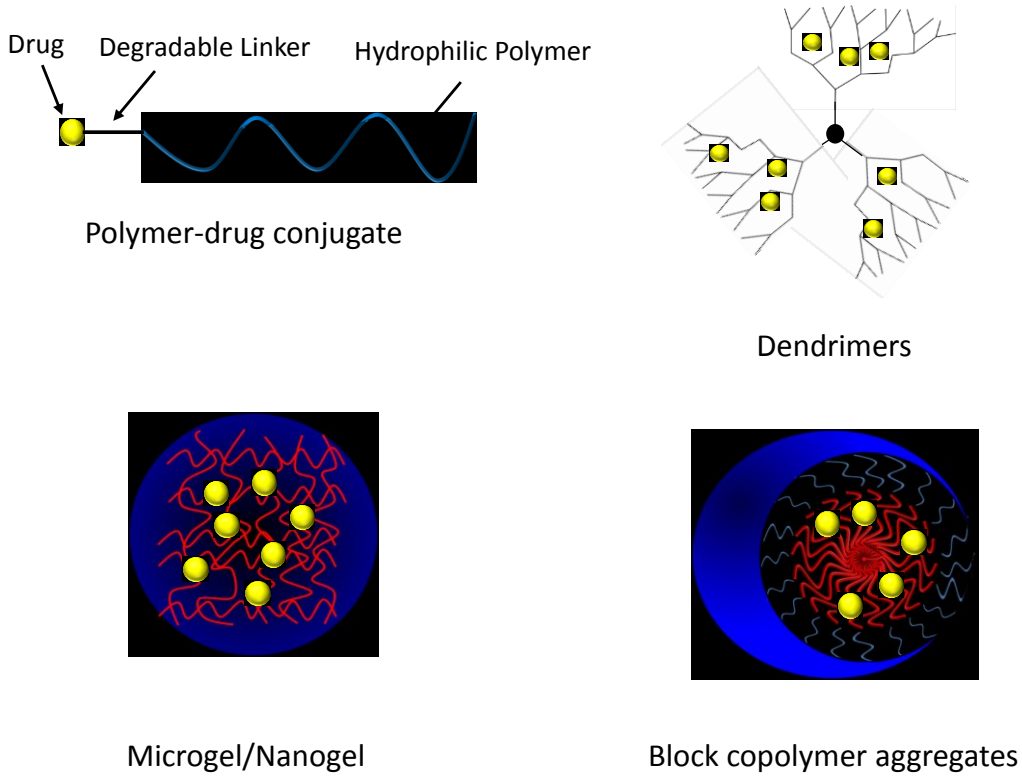

Figure 1.1. Different types of polymer-based DDS.

Polymer-drug conjugates, also referred to as polymer prodrugs, are an inactive form of a drug conjugated to a polymer where the drug is converted back to its active form upon cleavage of the bond that links the polymer to the drug.[7b] These polymers increase the water solubility of the drug, therefore enhancing their bioavailability. Moreover, they serve to protect the drug from deactivation and preserve its activity, while promoting cellular internalization through the use of ligands conjugated to the ends of the polymer.[10] In addition, the use of covalent bonds that may be enzymatically cleaved in specific cellular environment allows for the selective release of the drug. However, polymer-drug conjugates have a common limitation: the presence of various reactive groups on the drugs thereby complicating the conjugation task.[7b]

Similarly, dendrimers, highly branched macromolecules with many arms emanating from a core, offer promising properties for drug delivery applications.[11a] Prepared by a stepwise synthesis, they are composed of a highly regular branching pattern as opposed to the hyperbranched polymers characterized by irregular branching, albeit readily accessed by various facile polymerization strategies. On one hand, these structures offer certain advantages that include a multivalent architecture enabling the attachment of several drugs, targeting groups, and solubilizing groups in a well-defined manner.[11b] Moreover, their low-polydispersity in their synthesis allows for a batch-to-batch reproducibility which translates into reproducible pharmacokinetics. On the other hand, they suffer from inadequate drug release, when using enzymatically cleavable linkages, from these nanocarriers due to the steric hindrance.[11a] Their biodistribution is also challenging whereby issues in generating structures marked by prolonged circulation time whilst averting long-term buildup remains to be elucidated.

Hydrogels have also shown drug delivery applications. Either referred to as microgels, for micrometer-sized hydrogels or nanogels for nanometer-sized hydrogels, they are made up of water-soluble polymers that adopt a three-dimensional cross-linked network.[12a] They have various assets that justify their use in drug delivery; namely, a highly porous network which can be easily tuned by varying the amount of crosslinks. The porous structure of the hydrogels allows for loading of drugs into the gel matrix and their subsequent release which becomes limited by the rate of diffusion of these molecules throughout the pore network.[12b] Therewith, they can also be prepared from biocompatible materials and be designed to be biodegradable through the incorporation of stimuli-responsive groups. However, they also suffer from certain drawbacks: such as limitations in quantity and heterogeneity of drugs which may be loaded. Indeed, due to their high water content loading of hydrophobic drugs may be hindered.[12b] Moreover, their high porosity entails a rapid drug release which may be unwanted for certain applications.

My thesis work includes mainly ABP-based nanocarriers for drug delivery applications.

1.3.3 ABP-based drug delivery nanocarriers

As illustrated in Figure 1.2, ABPs are block copolymers which are composed of two or more covalently linked blocks that bear hydrophobic and hydrophilic properties. These block copolymers assemble into aggregates in aqueous solutions; the hydrophobic block constituting the core and the hydrophilic block the corona, thereby providing colloidal stability to the aggregates. Governed by an enthalpy driven process,[14] the resulting self-assembled aggregates exist in various morphologies, such as spheres, elongated spheres, rods, tubules, lamellae, and vesicles.[13] Their shape and size depends on

the balance of three forces acting on the system: 1) the constraints on the core-forming block (the block being stretched or contracted depending on the solvent); 2) the interaction between the corona-forming blocks; 3) the energy at the interface between the solvent and the core-forming block.[15] These forces are balanced by a number of morphological parameters which typically include block copolymer composition, copolymer concentration, temperature, copolymer architecture, and the nature of the solvent used for the micelle preparation.[14b]

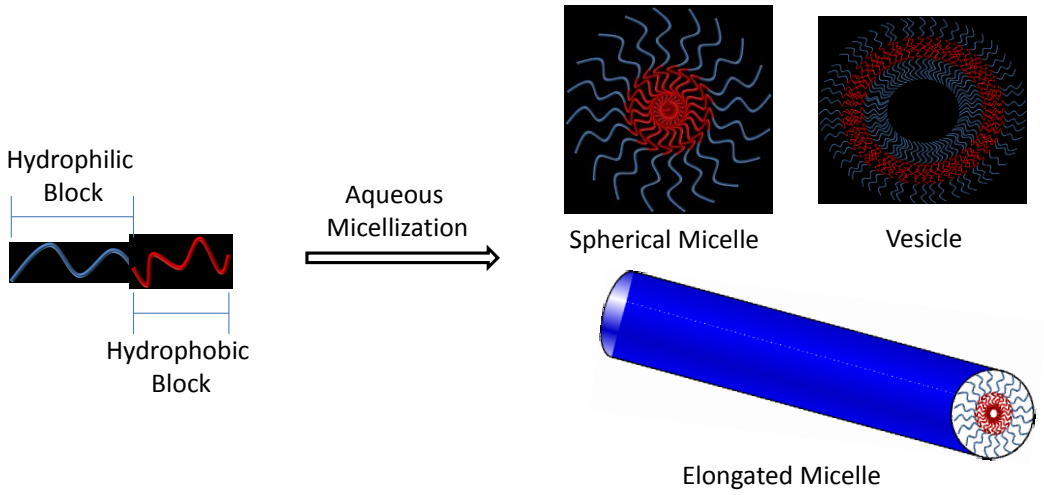

Figure 1.2. An illustration of aqueous self-assembly of ABPs into different aggregates.

1.3.4 Micellization of ABP

The topic of my master's research deals with the formation of spherical micelles, also referred to as micellar aggregates, for drug delivery applications, consequently this discussion is focused on the formation of micellar aggregates in aqueous solution. Governed by thermodynamics, micelles form when the concentration of amphiphilic block copolymers is above a certain concentration, known as the critical micellar concentration (CMC) and below a specific temperature, known as the critical micellar temperature (CMT).[14b, 15] When these ABPs are dissolved in water that is selective for the hydrophilic block, the ABPs

exist as unimers in aqueous solution. However, above a certain concentration the enthalpic cost arising from the contact of the hydrophobic block and the aqueous solution overcomes the entropic cost resulting in the aggregation of these ABP unimers in order to minimize the contact between the hydrophobic block and the aqueous solution.[14b] However, this phase separation is counter balanced by the repulsive forces in the hydrophilic blocks since these extend to hydrate themselves maximally. This equilibrium between these two forces generates these micellar structures that all have a certain curvature. If the concentration of these ABPs is further increased towards the semi-dilute to high concentrations, an arrangement of these micelles into an ordered state is obtained which leads to the process known as gelation.[16] Specifically for spherical micelles, there exist two types of micelles, crew-cut micelles and star-like micelles.[16] In the case of star-like micelles, the insoluble block is smaller than the soluble block and the resulting micelles have a small core and a long corona. Conversely, in the crew-cut micelles the core forming block is longer than the hydrophilic block such that the core is large and the corona is short.

Micelles are characterized by their thermodynamic and kinetic stability. The thermodynamic stability of a micelle pertains to its stability relative to its disassembly into single chains in solution.[15] On the other hand, upon dilution of the micelles below the CMC value, the micelles remain stable for some time before disassembling. Referred to as kinetic stability, this phenomenon depends on factors such as the physical state of the micelle core, where micelles formed by a hydrophobic block that has a high T_g will tend to disassemble more slowly.[15] Also, the length of both blocks, as well as the presence of hydrophobic molecules in the core affects this stability, where a micelle composed of an ABP with a large hydrophobic/hydrophilic ratio is portrayed with a lower rate of disassembly.

In the field of drug delivery application, the CMC is an important feature that impacts the propensity of the drug delivery system towards a successful application. Upon injection of a drug-loaded ABP in the human body a large volume of dilution arise. The average blood volume in an individual is approximately 5 L. If, for example, 100 mL of a 2.5% (w/w) micelle solution is injected, the concentration of the micelle solution falls to 0.5 mg/mL. Consequently, an ABP system with a low CMC is desired for drug delivery applications. Many factors govern the CMC, most notably the nature and length of the core-forming block, the length of the hydrophilic block, and the presence of hydrophobic solubilizates, such as hydrophobic therapeutic drugs.

1.3.4.1 Micelle size

In addition to surface charge and nature of hydrophilic corona, the size of micelles is an important characteristic with regards to drug delivery applications. The size of these ABP-based micelles can impact their circulation time and their biodistribution in the human body.[1] Particles circulating in the blood stream have their fate determined partly by their size. Particles that are larger than 200 nm are recognized by the reticulo-endothelial system (RES) and removed by macrophages, dendritic cells, or neutrophils.[17] Moreover, pertaining to drug delivery towards anti-cancer applications, the fenestrae of endothelial cells lining the blood vessels in tumor tissues are characterized with larger gaps than that in healthy tissues.[18] In addition, these tumor tissues are also characterized with poor lymphatic drainage due to poor development of a lymphatic system surrounding these tissues.[19] This increase in gap size for these endothelial cells lining the blood vessels and improper lymphatic drainage gives rise to a phenomenon referred to as the enhanced permeability and retention effect (EPR).[20] EPR, a passive and only targeting means in blood circulation, forms the basic mechanism by which nanoparticles escape from the blood circulation and enter these tumor

tissues. The large gaps between endothelial cells in the tumor vasculature allow large nanoparticles to escape the blood circulation, while the improper lymphatic drainage causes accumulation of these nanoparticles in the tumor tissue (Figure 1.3). As a result, this presents an advantage for targeting cancer cells since nanoparticles are designed to be large enough to avoid penetration in healthy tissues, but small enough to pass through these gaps in tumor blood vessels.

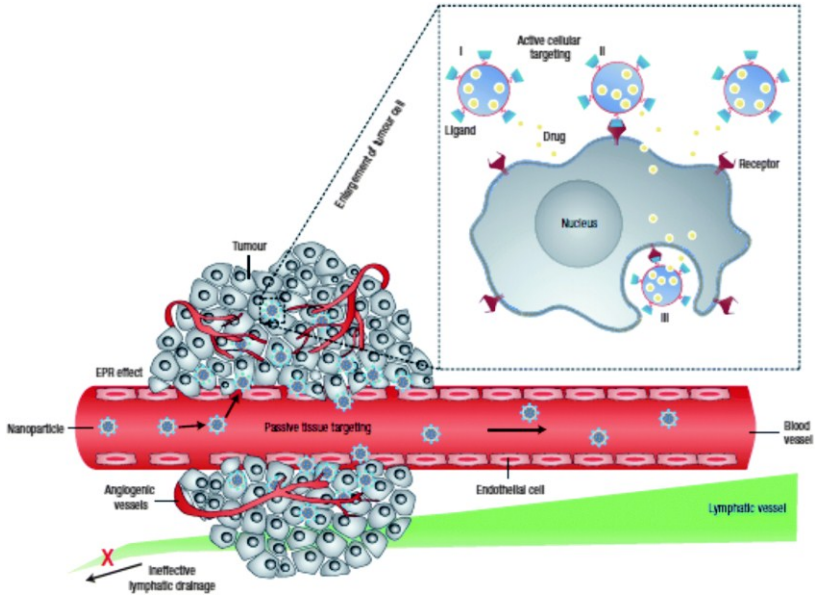

Figure 1.3. Drug accumulation into cancer tissues arising from the enhanced permeation and retention effect (EPR).[21]

1.3.5 Micelle preparation

To prepare these micelles into nanoparticles, various methods have been developed and they are an essential part for optimal delivery. The preparation methods fall within two categories: the one-step and two-step nanoparticle (NP) formation. In the one-step approach, an organic solution that contains the ABP and the drug is added drop-wise to an aqueous solution under stirring. The aggregates are formed instantly as polymer diffuse into the aqueous phase.[22] In this method, the organic and aqueous solutions are miscible. The parameters that

govern the particle size are the miscibility of the two solutions, the rate of addition, and the stirring speed.[23] Typically, aggregates formed through this method are smaller than the other methods, and this process may be applied to a wide range of materials.[22] For the two-step NP formation, there exist three different types of preparation methods; emulsification-solvent evaporation, emulsification-solvent diffusion, and emulsification-salting out. These methods rely on the formation of an oil-in-water emulsion. Here, the polymer and the drugs are dissolved in the organic phase, which appear as emulsion droplets, and the subsequent removal of the organic phase drives the formation of the nanoparticles. Depending on the emulsification process, the size and drug loading of the nanoparticles varies. However, in these preparation methods the drug loading are usually lower than for the one-step approach.[22]

In the emulsification-solvent evaporation technique, the most common preparation method for NPs, the solvent is removed through evaporation under reduced pressure following emulsification.[23] As the solvent evaporates the NPs are formed. This method is typically used for the encapsulation of lipophilic drugs and the size of the nanoparticles is influenced by the coalescence of emulsion droplets. In the emulsification-solvent diffusion technique, the organic phase, which is partially water-miscible, is removed through diffusion from the emulsion droplets into the water phase. In this method, due to the fast diffusion of the organic phase the physical properties of the NPs produced are reproducible and generally this method produces NPs with an average diameter of 150 nm.[23] In the emulsification-salting out method, the organic solvent used is totally water-miscible. However, the aqueous phase is saturated with a salt which prevents the mixing of the organic phase and the aqueous phase enabling the emulsion to form.[22] Then, the organic phase is removed by dilution with water which reduces

the salt concentration and allows mixing of the two phases. Typically, this method produces NPs that are smaller, but with lower encapsulation efficiency.[24]

1.4 Stimuli-responsive copolymers in drug delivery

In light of the previous sections, ABP-based DDS possess a number of advantages towards successful drug-delivery applications; these include low colloidal stability (low CMC), tunable and narrow size distribution, protection of drugs from possible deactivation during blood circulation, high loading efficiency of the drug without further chemical modifications, and bioconjugation of the delivery vehicle for targeted delivery in tissues or organs as well as cellular internalization. However, an ongoing challenge involve controlled/enhanced release of encapsulated biomolecules for DDS in targeted cancer cells after cellular uptake (i.e. endocytosis). A promising solution to circumvent this challenge can be found in stimuli-responsive degradation (SRD).[25] This promising platform for the efficient release of loaded therapeutic molecules finds its mainspring in the incorporation of dynamic covalent bonds in the architecture of polymers. These covalent bonds, in response to precise stimuli, are cleaved thereby disrupting the integrity of the structural conformation of the polymer. Appropriately positioned in the polymer backbone, these covalent bonds can cause disruption of the integrity of nanoparticles formed from these polymers in response to the stimuli, leading to the release of encapsulated drugs (Figure 1.4). Moreover, the incorporation of SRD allows for a morphological control on the nanoparticles in response to specific stimuli.

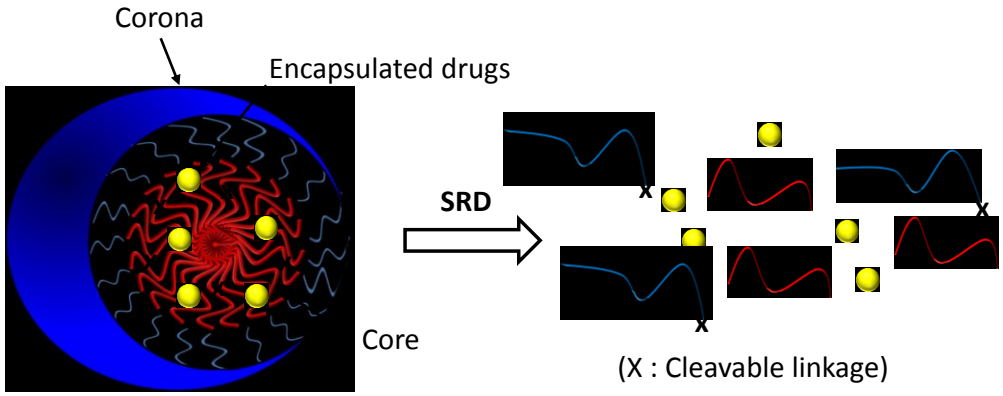

Figure 1.4. Stimuli-responsive degradation for the spatio-temporal release of encapsulated therapeutic drugs for block copolymer-based nanocarriers.

1.4.1 Stimuli-responsive covalent linkages

There exist numerous types of stimuli-responsive covalent bonds where the stimuli-responsive polymer undergoes physical or chemical changes in response to the stimuli. For example, acid-labile acetals, orthoesters, imine, and hydrazone linkages can be cleaved in acidic pH.[26] Coumarin dimers, 2-diazo-1,2-napthoquinone, and *o*-nitrobenzyl linkages can be cleaved in response to light.[27] Moreover, the use of ultrasound-responsive and enzymatically cleaved linkages have been explored for their use in drug delivery applications.[28] In my master's research, the thiol-responsive disulfide linkage was examined for its potential in drug delivery applications for anti-cancer therapeutics.

Disulfides are promising in that they are cleaved through a disulfide-thiol exchange reaction in the presence of free thiols as reducing agents.[25, 29] In biological systems, glutathione (GSH), a tripeptide formed by glutamic acid, cysteine and glycine, is a cellular reducing agent that cleaves disulfide linkages, and is found at higher concentrations of its reduced state in intracellular environments in comparison to the extracellular milieu.[30] Moreover, GSH is

found at elevated levels in numerous types of cancerous cells through the up-regulation of the enzyme glutathione disulfide reductase which catalyzes the reduction of GS-SG into GSH.[31] Therefore, the reduction-responsive disulfide is a promising platform in the construction of reduction-responsive degradable ABP-based nanocarriers for tumor-targeted drug delivery applications.

1.4.2 Approaches to preparation of reduction-responsive micelles at different locations

Disulfide linkages can be positioned at different locations and with different quantities in the polymer structure leading to different outcomes upon degradation. There are five main categories for the location of these disulfide bonds which are presented in Figure 1.5.[25] In general, the main approach to elicit the degradation of ABP-based micelles in response to reductive reactions is through the tuning of the hydrophobic-hydrophilic balance by removing one of the blocks.[32]

In strategy A, the disulfide linkage is incorporated between the hydrophobic and hydrophilic blocks such that in response to free thiols as reducing agents the hydrophilic corona is shed from the micelles thereby disrupting the colloidal stability and causing the release of the encapsulated drug.[25, 33] For example, an ABP-based drug delivery nanocarrier was labeled with a disulfide linkage at the interface of hydrophobic polylactide (PLA) and hydrophilic poly[oligo(ethylene glycol) monomethyl ether methacrylate] (POEOMA) for controlled/enhanced drug release.[33b] These ABPs formed colloidally stable micelles with PLA as the core and POEOMA as the corona. Thiol-responsive degradation resulted in the shedding of the POEOMA corona causing PLA to precipitate, thereby showing their potential as drug delivery nanocarriers.

Strategy B involves multiple disulfide linkages positioned as pendant chains in the hydrophobic block. Upon cleavage of the disulfides, the polarity of the hydrophobic block is increased thereby causing the micelles to disintegrate which ultimately leads to the release of the loaded drugs.[34]

Strategy C involves multiple cleavable linkages positioned repeatedly in the polymer backbone of the hydrophobic block.[35] In response to the stimuli, the hydrophobic block becomes destroyed and the micelles are broken down. For example, block copolymer micelles composed of a polyester as hydrophobic block labeled with repeating stimuli-responsive disulfide linkages, and a polymethacrylate as hydrophilic corona were synthesized.[35a] The disulfide linkages were cleaved in the presence of thiols to enhance the release of loaded molecules.

Finally, in strategy D monocleavable ABP with the stimuli-responsive group in the middle of triblock copolymers are shown. In these systems, the stimuli-responsive group is found in the core of the micelle and upon cleavage the resulting block copolymer retains amphiphilicity.[36] Such a process enables a change in the size of the monocleavable micelles. There has been a limited number of reports that describe methods to synthesize these monocleavable ABPs, using thiol-alkyne click reactions,[37] ROP,[38] ATRP,[36b] or reversible addition-fragementation chain transfer (RAFT).[39] As a result, in this thesis different synthetic strategies will be studied for the preparation of monocleavable ABPs.

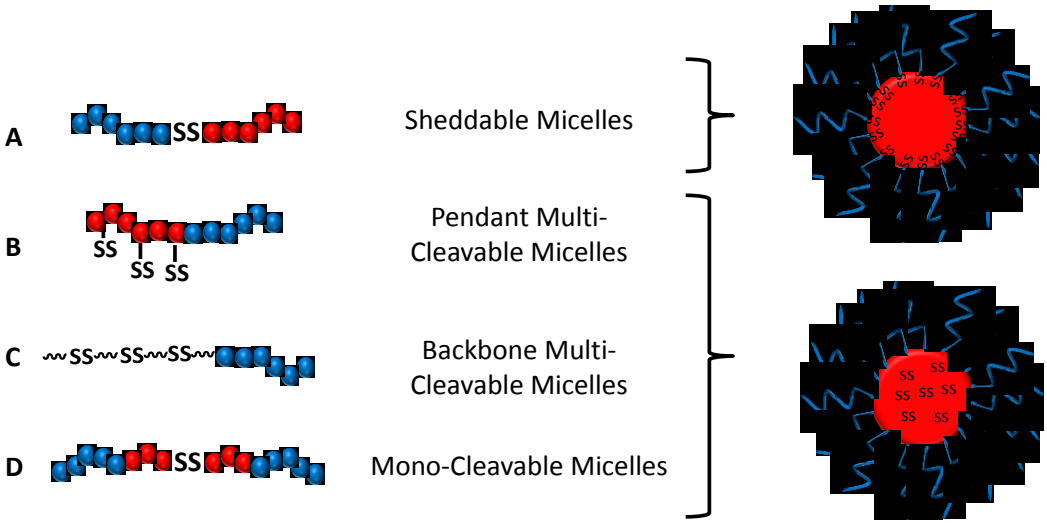

Figure 1.5. Approaches to synthesis of disulfide-containing block copolymers and their self-assembled disulfide-labeled aggregates with different numbers and position.[25, 40]

1.5 Biocompatible polylactide and their nanomaterials

1.5.1 Polylactide and its challenges in biomedical applications

The biomaterial of choice for my research is poly(D,L-lactide) (PLA) (Figure 1.6). PLA is a class of hydroxyalkanoic acid-based hydrophobic aliphatic polyesters, along with polycaprolactone (PCL) and polyglycolic acid.[41] PLA shows tunable mechanical properties[42], biodegradability through hydrolysis of the ester bonds or enzymatic degradation via proteinase K,[43] and biocompatibility.[44] PLA has been FDA-approved for its clinical use. Because of these advantageous properties, PLA has found numerous applications, namely in drug delivery,[45] as tissue scaffolds,[46] and as nanocrystal-embedded imaging platforms.[47]

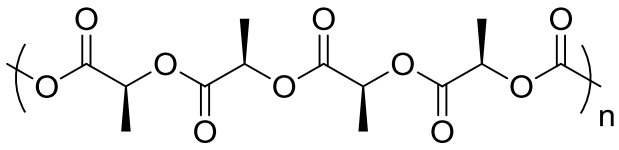

Figure 1.6. D,L-polylactide.

Although PLA has numerous advantages rendering it a promising platform as a material of choice for the development of biomedical applications, there are two main limitations that need to be addressed to promote commercial value of PLA-based drug delivery systems.[48] The first limitation involves its inherent hydrophobicity.[49] PLA is hydrophobic and therefore if injected inside the bloodstream, this aqueous environment will cause its aggregation and precipitation of the polymer. These aggregates can be recognized as foreign materials and be cleared by the reticulo-endothelial system (RES); a component of the immune system consisting of phagocytic cells. To circumvent this limitation two strategies have been proposed. One strategy is to functionalize PLA with a hydrophilic polymer in a copolymer architecture which allows the preparation of self-assembled nanoparticles with the hydrophobic PLA as a core and reservoir and the hydrophilic polymer as a corona surrounding the PLA core and providing colloidal stability.[48] The other approach involves the copolymerization of PLA with hydrophilic monomers to form microparticles that have the ability to encapsulate the therapeutic molecules of choice, while still rendering PLA less hydrophobic.[50]

The other limitation is the slow biodegradation of PLA. Although PLA is biodegradable via hydrolysis of the ester bonds or enzymatic cleavage using Proteinase K, the degradation process is slow. Indeed, the hydrolysis of the ester bonds occurs via a bulk erosion mechanism, whereas PLA is hydrophobic and does not permit adequate hydrolysis of the interior of the polymer matrix to

facilitate its degradation.[44] Due to this slow degradation, PLA-based drug delivery systems are characterized by a slow and uncontrolled delivery of the loaded therapeutics.[51] A promising solution to improve the release is to introduce SRD platform in the design of PLA-based drug delivery systems, which has been proposed by Prof. Oh's research group. With promising disulfide-thiol chemistry, our group has continued to put significant efforts to develop a variety of disulfide containing PLA-based ABPs. Examples include sheddable micelles and fibres having disulfides located at block junction of diblock copolymers,[33b, 52] as well as inter-layered crosslinked micelles having disulfide linkages positioned at dual locations of a triblock copolymer.[53] A promising and interesting system is the monocleavable micelle having disulfide linkages in the middle of PLA-based triblock copolymers. Because few reports have been directed at the study of this system, the disulfide-labeled monocleavable triblock copolymer was studied in order to gain a greater insight on the structure-property relationship between this morphological variance and its impact on the stimuli-responsive degradation. The prospect held by this architecture for efficient drug delivery is outlined in the belief that retaining amphiphilicity post-drug release allows for a safe removal of the empty delivery agents. Numerous drug delivery methods either result in the formation of hydrophobic aggregates following stimuli-responsive degradation or rely on the dissolution of the copolymer chains. Potential toxicity issues may arise under these circumstances which may be averted by exploiting this monocleavable system.

1.5.2 Literature related monocleavable micelles

This section is to briefly summarize strategies to synthesize monocleavable micelles reported in the literature. In one example, a thiol-alkyne click reaction was used to prepare mPolycaprolactone-*b*-Polyehtylene oxide (mPCL-*b*-PEO) multi-armed biodegradable block copolymers with the disulfide

bond in the core.[37] The srategy was based on the click reaction between an alkyne-terminated, disulfide-labeled linker and a thiol-terminated PEG-*b*-PCL diblock copolymer which gave rise to monocleavable ABP with the disulfide bond in the core. These ABPs assembled into bioreducible micelles that presented thiol-triggered drug release properties. In presence of thiol-reducing agents, the micelles showed a reduction in size, without alterations in their morphology, and an improvement of drug release. In another strategy, a dual stimuli-sensitive star polypeptide was synthesized with a disulfide bond in the middle of the star.[38] The four branched star-liked structure was prepared using a disulfide-bond-cored tetra(amine) as an initiator for the ring-opening polymerization (ROP) of diethylene glycol-L-glutamate *N*-carboxyanhydride. The resulting disulfide-labeled ABP were able to form micelles in aqueous environment and showed stimuli-responsive drug release properties. Moreover, a different strategy employed a combination of reversible-addition fragmentation chain transfer (RAFT) and ROP to prepare star-like terpolymers.[39a] In this example, the strategy was based on first using a disulfide-labeled RAFT agent for the sequential polymerization of vinyl-benzyl terminated polyethylene gycol (St-PEG) followed by *N*-(2-hydroxyethyl) maleimide (HEMI). Then, the terminal hydroxyl ends of HEMI were used as initiators for the ROP synthesis of PCL. The resulting synthetic strategy gave rise to a mid-disulfide-linked comblike copolymer of the form S-CP(PEG-*alt*-PCL) which were then studied for their potential as drug delivery systems.

In light of all the previously discussed advantages confered by the combination of ABP and SRD strategies in the design of drug delivery systems, the proof of concept based on these systems has made its mark. Indeed, a great deal of effort has been directed towards understanding the necessary components of a successful drug delivery system and the SRD platform is the missing link. In

retrospect, albeit not a challenge to the central tenet brought about by Paul Erlich`s magic bullet but merely a humble observation of the current situation, little progress has been made from the benchtop to a prescribed ABP-based drug. This observation stems from the tremendous amount of literature that deal on ABP-based drug delivery system, but the scarce amount of prescribed drugs that utilize this concept. Part of the answer to this observation may be found in the inadequate understanding between the structure-property relationship between morphological variance and stimuli-responsive degradation. A greater understanding would enable the optimization of the design of these delivery systems. Moreover, another deficiency in our progress is the development of synthetic methods that allow a reproducible and cheap synthesis of these ABP-based systems to render the commecialization of these products feasible and attainable. The topic of my research has been directed toward the development of different synthetic strategies to prepare PLA-based disulfide-labeled monocleavable triblock ABP. To the best of my knowledge, there are no reports that propose a synthetic strategy of disulfide-labeled linear triblock copolymers which use PLA as the hydrophobic block. Moreover, the impact of this morphology on the SRD and corollary drug release was studied. Different synthetic strategies were proposed in order to augment the possible combination of hydrophobic and hydrophilic polymers that can be used to form the monocleavable triblock ABP. Finally, their potential as drug delivery systems were studied to give a greater insight of the use of this morphology and the use of the disulfide bond in drug delivery applications.

1.6 Scope of the thesis

In this thesis, the research conducted and results obtained are described in three chapters. In chapter 2, the synthesis and characterization of PLA-based

ABPs and their self-assembled nanostructures are presented along with the relevant background information.

In chapter 3, the novel synthesis of well-defined reduction-responsive degradable PLA-based micelles having disulfide linkages in the middle of triblock copolymers is reported. The proposed ABP was synthesized by a combination of a facile controlled polymerization technique, atom transfer radical polymerization (ATRP) and ring-opening polymerization (ROP). The central disulfide linkages were cleaved in response to thiols, enhancing release of encapsulated anticancer drugs.

In chapter 4, another synthetic method for the preparation of monocleavable micelles is presented. The approach combines the use of ROP and a facile coupling reaction to prepare an ABP composed of biocompatible and FDA-approved polymers, polyethylene oxide (PEO) and PLA. In addition, the proposed PEO-b-(PLA-SS-PLA)-b-PEO triblock copolymer was evaluated for its prospective drug delivery applications. Indeed, PEO has been found to be the ideal hydrophilic block in the design of drug delivery systems exhibiting enhanced colloidal stability and preventing non-specific protein interactions. Further, thiol-triggered release enabled the enhanced drug release in response to glutathione, a cellular trigger.

Finally, the concluding remarks and future perspectives are discussed in chapter 5.

Chapter 2

Methodology: Synthesis and Characterization

2.1. Brief description

This chapter describes the methodology used for the synthesis and characterization of the monocleavable triblock copolymers and their self-assembly driven aggregation into micelles, as well as the techniques used to determine their biological and biomedical applications. Their detailed experimental procedure are described in chapter 3 & 4 (Experimental).

2.2 Synthesis and characterization of triblock copolymers

2.2.1 ROP for the synthesis of PLA

In order to be used in biomedical applications, polymers and copolymers need to have a small population distribution. Hence, a precise and stringent control on their polymerization is necessary. To obtain an amphiphilic triblock copolymer, PLA was used as the hydrophobic block. There have been various methods that have been developed to synthesize PLA.[54] Most notably, a direct polycondensation polymerization of lactic acid in the presence of a catalyst under reduced pressure affords PLA.[54] However, this method suffers from certain drawbacks in that the polymers obtained have a low molecular weight due to the difficulties of removing water from the viscous mixture as it is generated and the stereoregularity cannot be controlled during the course of the reaction.[54] Variants of this method are azeotropic condensation polymerization that affords polymers with large molecular weights, and solid state polymerization that offer a rigorous

control over side reactions. Another method that most widely used to synthesize PLA is the ring opening polymerization.[41, 54-55] Demonstrated by Carothers et al. in 1932, this method offers control of the PLA chemistry and properties, as well as their stereoregulation.[41, 54-55] Here, the monomers are the cyclic dimers of lactic acid. There exist three types of ROP based on their reaction mechanism: anionic, cationic, and coordination-insertion mechanism.[54] In the anionic polymerization, a nucleophilic anion attacks the carbonyl carbon and results in the cleavage of the carbonyl carbon and the endocyclic oxygen. These polymerizations are characterized by racemization, back biting and other side reactions due to the presence of highly active catalysts at high temperatures (Figure 2.1).[56] In the cationic polymerization, an exocyclic oxygen of the lactide monomer is either alkylated or protonated causing the resulting oxygen to become positively charged, followed by subsequent nucleophilic attacks by the acidic initiator to cause the ring-opening (Figure 2.1).[54]

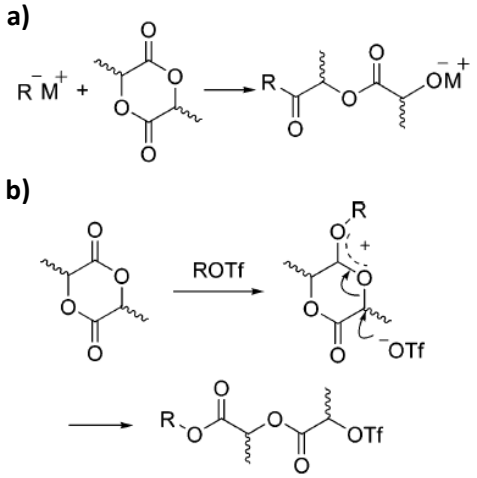

Figure 2.1. Scheme for the (a) anionic ROP of LA and (b) cationic ROP of LA in the presence of methyl trifluoromethanesulfonate (MeOTf).[55]

Similarly, due to the high temperature requirements, racemization is often encountered. Finally, the ROP method that was used in this research is the coordination-insertion mechanism which is the most widely used for the synthesis of high molecular weight PLA with well-defined molecular weight and stereoregulation. As depicted in Figure 2.2, the first step of the polymerization is the coordination of oxygen of the initiator with the metal atom found on the catalyst.[55, 57] This coordination increases the nucleophilicity of the oxygen. Then, the exocyclic oxygen of lactide is coordinated with the metal atom displacing the alkoxide initiator which then attacks the lactide at the carbonyl carbon followed by ring opening. This two step-attack and ring opening result in the insertion of a monomer into the OH bond of the initiator. These steps are repeated until all monomers are exhausted. A great deal of catalysts have been studied for the ring opening polymerization of lactide, however in this research the Tin(II) 2-ethylhexanoate ($Sn(Oct)_2$) catalyst has been used because it is soluble in many organic solvents, it is efficient and provides high conversion and reaction rates.

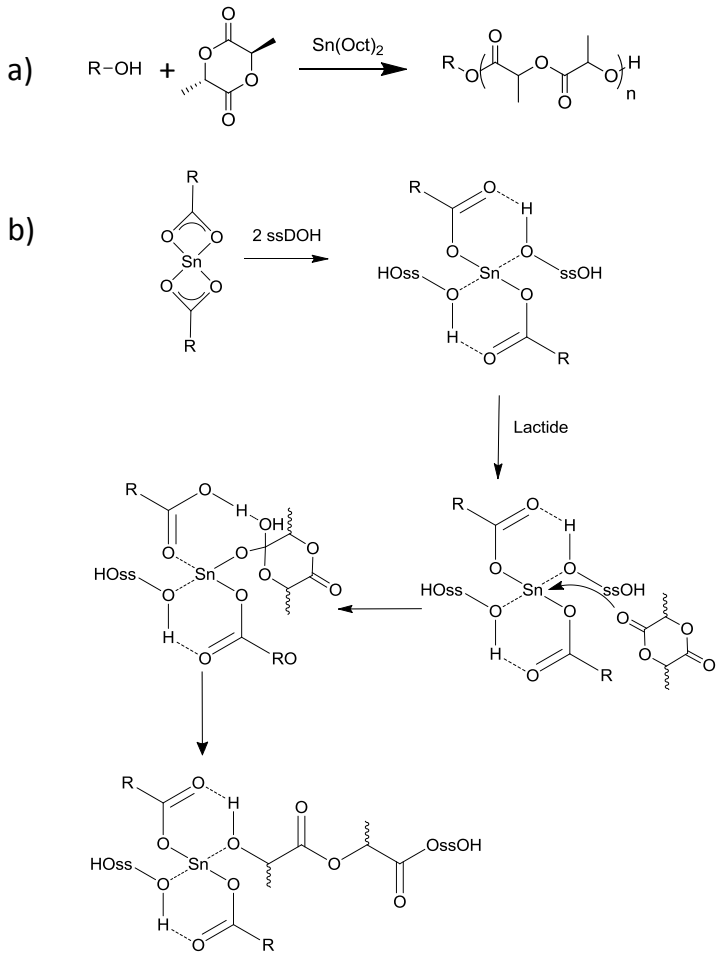

Figure 2.2. Scheme (a) and mechanism (b) for the coordination-insertion ROP of LA in the presence of $Sn(Oct)_2$.[55]

2.2.1 ATRP for the synthesis of ABP

Another polymerization technique that allows the synthesis of well-controlled polymers and copolymers with a narrow molecular weight distribution and various architectures is ATRP. Independently discovered by both Mitsuo Sawamoto[58] and by Jin-Shan Wang and Krzysztof Matyjaszewski[59] in 1995, this technique falls in the category of controlled radical polymerization. This polymerization method relies on the propagation of a radical active chain end.

Due to the presence of the radical species as propagating centers, this type of polymerization is limited to monomers that contain substituent groups that can stabilize the propagating radicals, such as styrenes, acrylates, acrylamides, and acrylonitrile.[60] ATRP finds various applications, notably in the synthesis of ABP for biomedical applications due to its numerous advantages: 1) synthesis of well-controlled polymers with predetermined molecular weights and low polydispersity; 2) synthesis of polymers with various topologies; 3) synthesis of copolymers with different compositions; 4) synthesis of polymers with different terminal functional groups, which can be used, for example, to couple ligands for receptor-mediated endocytosis in specific cells.

As depicted in Figure 2.3, ATRP relies on equilibrium between actively propagating chains and dormant chains. In ATRP, a halogen atom undergoes a reversible, homolytic halogen transfer from an initiator species to a transition metal complex in its lower oxidation state.[61] This activation, characterized by the rate constant (k_{act}), generates active radical chains ends. Monomers are sequentially added to this radical chain end by which polymer chains grow. This propagation is characterized by the rate constant (k_p). The propagation ends either through reversible deactivation with a rate constant k_{deact} or by undesired irreversible termination reactions with a rate constant k_t. By keeping the concentration of dormant species higher than the concentration of active species, the amount of irreversible termination reactions is diminished ($k_{deact} >> k_{act}$). Moreover, $k_{act} > k_p$ such that all chains are propagating at the same time aiding in the generation of polymers with narrow molecular weight distribution.

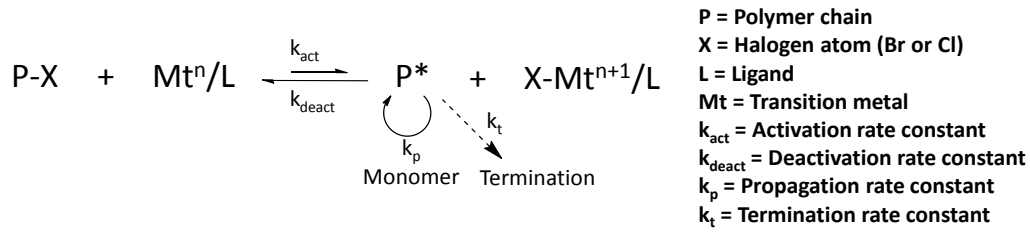

Figure 2.3. Mechanism for ATRP polymerization.[62]

2.2.2 Copolymer characterization: Gel permeation chromatography (GPC)

Polymers are characterized by population distributions. In order to better depict this population distribution and understand their properties polymers are reported according to their number-average molecular weight (M_n), weight-average molecular weigth (M_w), and polydispersity index (PDI). The M_n is the number-average molecular mass of the polymers present in the sample according to the number fraction of polymer chains and is defined by: $M_n = (\Sigma N_i M_i)/(\Sigma N_i)$, where N_i is the number of polymer chains and M_i is the weight or weight class for a polymer. On the other hand, the M_w is the weight-average molecular mass of the polymers present in the sample according to the weight fraction of these polymer chains and is defined by: $M_w = (\Sigma N_i M_i^2)/(\Sigma N_i M_i)$. Finally, the PDI is a measure of the dispersity of the population such that a PDI of 1 indicates a monodisperse population. The value for the PDI may be obtained from the following: PDI = M_w/M_n.

Gel permeation chromatography (GPC) is a convenient method to determine relative (not absolute) molecular weight data. GPC separates polymer chains with respect to their hydrodynamic volumes, which itself depends on the molecular weight and molecular conformation of the polymer in solution. In this case, a polymer solution is injected inside the instrument where an eluent (mobile phase and good solvent for the polymer) carries the polymer through columns

filled with porous beads. At the end of the column, a detector measures the refractive index monitors the concentration by weight of polymer solution that elutes from that column. Polymer chains are separated based on their hydrodynamic volume by interaction with the porous beads. Short polymer chains may enter these pores and spend more time to travel across the column and reach the detector, whereas long polymer chains with a large volume are too big to interact with these pores and elute first. The time point at which these polymers elute is referred to as either the retention time or volume. By constructing a calibration curve with the known calibration standards of pre-determined molecular weight, the relative molecular weight of the polymer is determined. The typical calibration standards available include polystyrene (PSt) and poly(methyl methacrylate) (PMMA).

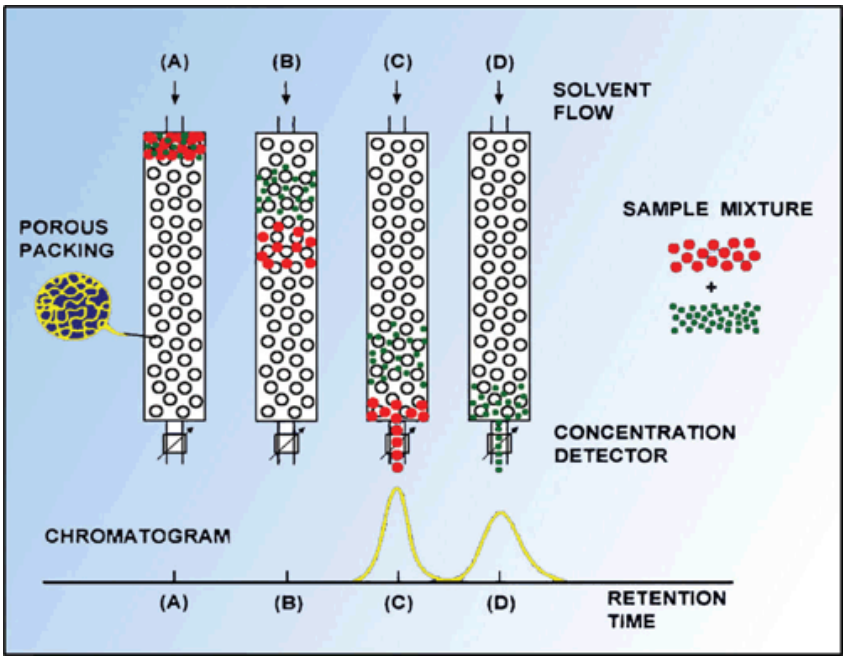

Figure 2.4. Principle for separation of polymers according to hydrodynamic volume.[63]

2.3 Aqueous micellization and characterization

2.3.1 Preparation of micellar aggregates

As discussed in section 1.3.5, various techniques for the preparation of micelles have been developed and allow nanoparticles of different sizes to be prepared using polymers with different properties.[22] The two methods that were mainly used in this research are the emulsification-solvent evaporation technique and the dialysis technique. In the solvent evaporation technique the ABP is dissolved in a volatile solvent, here THF, and mixed with deionized water. Formation of the NP is achieved as the solvent is evaporated and the ABP comes together in a thermodynamically driven aggregation to minimize contact of the hydrophobic block with water.[49c] The parameters affecting the NP formation are the evaporation temperature and pressure.[13] In the second method, the ABP is dissolved in a water-miscible solvent, here *N,N*-dimethylformamide (DMF), and transferred to a semi-permeable membrane. This solution is dialyzed against water with the dialysis bag preventing the micelles from diffusing out of the membrane. As the solvent is gradually replaced with water, micelles are formed.[49c]

2.3.2 Determination of critical micellar concentration (CMC)

As discussed in section 1.3.4, the CMC is the concentration of ABP above which micellar particles form in a thermodynamically driven self-assembly.[15] There exist different methods based on physical or chemical concepts to determine the CMC of an ABP-based micelle. Typical methods based on physical concepts include tensiometry, which measures changes in surface tension of a polymer solution as the concentration of polymer is increased, or electrical conductivity, which measures increases of electrical conductivity as ionically charged surfactant concentration is increased.[64]

On the other hand, chemically-based methods have been developed which utilize fluorescent probes such as Nile Red (NR)[65] or pyrene.[66] In this research, fluorescence spectroscopy using NR as a probe was used to determine the CMC of the ABP. NR is a solvatochromic probe that undergoes a shift in its emission spectrum based on the environment in which it is found.[65] Typically, NR undergoes a twisted-intramolecular chain transfer upon excitation where ground state electrons are excited to higher energy levels.[67] Then, these electrons will populate degenerate excited states based on the environment in which NR is found. These excited states are high in energy and can be stabilized in a polar environment such that depending on the polarity of the environment in which NR is found, different excited states with different energies are populated.[68] These different excited states will then emit fluorescence energy which can be measured with the help of a fluorimeter. By measuring the changes in fluorescence intensity at a specific emission wavelength the environment of the NR probe can be followed.[68] At this wavelength, when NR is in an aqueous environment, the fluorescence intensity is quenched due to its poor water solubility. However, once NR is encapsulated in the hydrophobic core of the micelle, the fluorescence intensity at this wavelength increases with respect to concentration.[68] Therefore, by preparing different polymer solutions at different concentrations and allowing them to form micelles using the emulsification-solvent evaporation technique in the presence of NR, the CMC can be obtained by observing the concentration of ABP at which there is an onset of fluorescence emission measured.

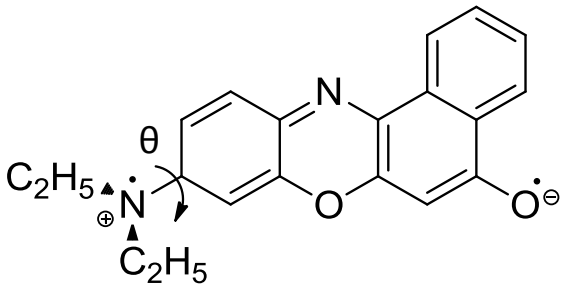

Figure 2.5. Twisted intramolecular chain transfer leading to NR excited state.

2.3.3 Size and morphology characterization

Dynamic light scattering (DLS) is a common technique that allows analyzing the size of colloidal dispersions. For the DLS measurements, incident light is directed to the cuvette containing colloidal dispersions when colliding with particles. The intensity of the scattered light is measured using appropriate optical arrangements. Note that the light scattering intensity of particles is inversely proportional to the size of the molecules. The integrated intensities of the particles in the dispersion are fitted to a valid mathematical model. From this model, the translational diffusion coefficient (D) is obtained and used to calculate the hydrodynamic diameter (d (H)) of the particles using the Stokes-Einstein equation.

Stokes-Einstein equation:

$$d(\mathrm{H}) = k\mathrm{T} / 3\pi\eta D$$

where, k is the Boltzmann's constant, T is the absolute temperature of measurement, and η is the viscosity of the medium.

Imaging techniques such as transmission electron microscopy (TEM) are used to investigate particle morphologies. For TEM, a specimen is loaded onto a sample holder and a beam of electrons is transmitted through this specimen. Then,

electrons interact with the sample on the specimen or pass through and the image that is observed is the electrons that have passed. Typically, the specimen used for TEM is a copper grid onto which a sample is deposited.

Chapter 3

New design of thiol-responsive PLA-based triblock copolymer micelles

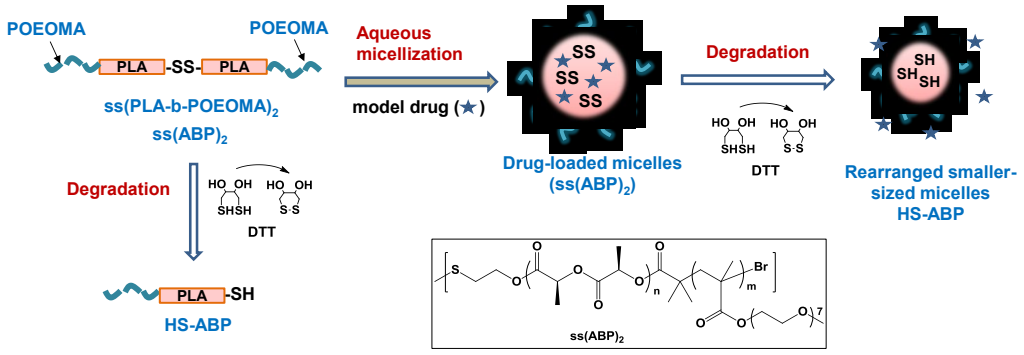

A new design to synthesize reduction-responsive degradable PLA-based micelles having a disulfide linkage in the middle of triblock copolymers (ssABP-1) is presented in this chapter. They were synthesized by a new method that centers on the use of a disulfide-labeled diol as an initiator for ring opening polymerization, followed by controlled/living radical polymerization. These well-controlled copolymers with monomodal and narrow molecular weight distribution ($M_w/M_n < 1.15$) self-assembled, through aqueous micellization, to form micellar aggregates with disulfide-containing PLA cores, which is not toxic to cells. Central disulfide linkages were cleaved in response to thiols; such thiol-triggered degradation enhanced the release of encapsulated anticancer drugs.

This chapter contains information that was published in *Macromolecular Rapid Communication*, **2013**, *34*, 163-168 and part of the chapter is reproduced from the article with permission from the publisher.

3.1 Introduction

Polylactide (PLA), a member of the class of hydroxyalkanoic acid-based hydrophobic aliphatic polyesters,[41] is biocompatible,[44] FDA-approved for clinical use, and biodegradable through enzymatic reactions and hydrolysis in physiological conditions.[43] These unique properties have recently facilitated its use in a variety of biomedical applications including drug delivery carriers,[45] tissue scaffolds,[46] and nanocrystal-embedded imaging platforms.[47] Toward the successful biological applications of PLA and its copolymers, a challenge involves their hydrophobicity.[49a, 49b] In general, hydrophobic PLA copolymers are modified with hydrophilic polymers[48] or copolymerized with hydrophilic monomers.[50] This approach has been facilitated by preparing PLA-containing amphiphilic block copolymers typically with hydrophilic polymethacrylates.[48] The resulting PLA-based block copolymers form self-assembled micellar aggregates in aqueous solutions, consisting of hydrophobic PLA cores surrounded with hydrophilic coronas. Another critical challenge to be addressed is the slow degradation of PLA and thus slow and uncontrolled release of encapsulated drugs.[51] Such slow release is attributed to delayed diffusion through the hydrophobic PLA core due to both hydrophobic interactions as well as the slow hydrolysis of the ester linkages of the PLA backbones. Several approaches including hydrolytic degradation at low pH[69] and mixed micelles with pH-responsive block copolymers[70] have been proposed; however, strategies toward a rapid and controlled degradation and release remain limited.

Stimuli-responsive degradation (SRD) is a desired property in constructing multifunctional nanocarriers.[25] SRD in response to external triggers enables not only enhancing the release of encapsulated biomolecules[28, 32, 71] but also tuning the morphologies of self-assembled nanostructures.[72] In general, stimuli-responsive cleavable linkages are incorporated into block copolymer micelles.

These linkages are then cleaved when they are triggered by low pH, light, or ultrasound, as well as reductive, oxidative, or enzymatic reactions, causing the nanomaterials to dissociate. Disulfide-thiol degradation is a promising SRD platform because disulfide linkages are cleaved to the corresponding thiols in response to reductive reactions.[29] Moreover, glutathione (GSH, a tripeptide containing cysteine and a reducing agent for disulfide linkages) is found at a higher concentration in intracellular environments than in extracellular environments,[30] and even at elevated levels in cancer cells.[31a, 31c] These features promote the use of the degradation platform for the development of self-assembled micellar aggregates labeled with disulfide linkages as enhanced/controlled delivery nanocarriers.[35d, 73]

In this chapter, a new method for the preparation of thiol-responsive degradable PLA-based triblock copolymer micelles exhibiting enhanced drug release will be presented. These micelles consist of well-controlled, monocleavable PLA-based amphiphilic triblock copolymers having a single central disulfide linkage in the middle of the hydrophobic block (called ssABP-1). These thiol-responsive block copolymers were synthesized by a combined method of ROP and ATRP; the method initiates the use of a disulfide-labeled diol as a ROP initiator. Then, they were characterized for aqueous micellization and thiol-responsive degradation. Well-controlled ssABP-1 self-assembles to form aqueous micellar aggregates. In response to thiols, the central single disulfide linkage in micellar core is cleaved, resulting in degradation of ssABP-1 to HS-ABP that retains amphiphilic character, thus causing micellar aggregates to change their sizes. Such thiol-triggered degradation enhances the release of encapsulated drugs.

3.2 Experimental

3.2.1 Instrumentation and analyses

^{1}H-NMR spectra were recorded using a 500 MHz Varian spectrometer. The $CDCl_3$ singlet at 7.27 ppm was selected as the reference standard. Spectral features are tabulated in the following order: chemical shift (ppm); multiplicity (s - singlet, d - doublet, t – triplet, m - complex multiplet); number of protons; position of protons. Molecular weight and molecular weight distribution were determined by gel permeation chromatography (GPC) with a Viscotek VE1122 pump and a refractive index (RI) detector. Two PolyAnalytik columns (PAS-103L, 106L, designed to determine molecular weight up to 2,000,000 g/mol) were used with THF as an eluent at 30 °C and at a flow rate of 1 mL/min. Linear polystyrene standards were used for calibration. Aliquots of polymer samples were dissolved in THF and the clear solutions were filtered using a 0.25 μm PTFE filter to remove any THF-insoluble species. A drop of anisole was added as a flow rate marker. Conversion for ATRP of OEOMA was also determined using GPC by following the decrease of macromonomer (OEOMA) peak area relative to the increase of polymer peak area. The sizes of micelles in hydrodynamic diameters by volume were measured by dynamic light scattering (DLS) at a fixed scattering angle of 173° at 25 °C with a Malvern Instruments Nano S ZEN1600 equipped with a 633 nm He-Ne gas laser. All micellar dispersions without dilution were filtered by 0.45 μm PES filter to remove large aggregates. Fluorescence spectra were recorded on Varian Cary Eclipse Fluorescence spectrometer using a 1-cm wide quartz cuvette.

3.2.2 Thermal analysis

Thermal properties including glass transition temperature (T_g) of ss(PLA-Br)$_2$ and ssABP-1 were measured with a TA Instruments DSC Q10 differential scanning calorimeter over a temperature range of -70 to 200 °C at a heating rate of 10 °C/min (cycles: cool to -70 °C, heat up to 200 °C (1st run 1), cool to -70 °C, heat up to 200 °C (2nd run), and cool to 25 °C). The T_g values were determined from the 2nd heating run.

3.2.3 Materials

2-Hydroxyethyl disulfide (ssDOH), α-bromoisobutyryl bromide (Br-iBuBr), triethylamine (Et_3N), 3,6-dimethyl-1,4-dioxane-2,5-dione (DL-lactide, LA), tin(II) 2-ethylhexanoate (Sn(Oct)$_2$, 95%), *N*,*N*,*N*′,*N*″,*N*″-pentamethyldiethylenetriamine (PMDETA, >98%), Nile Red (NR), potassium phosphate monobasic (KH_2PO_4), methanol (MeOH), and copper(I) bromide (CuBr, >99.99%) from Aldrich, and DL-dithiothreitol (DTT, 99%) from Acros Organics were purchased and used as received. Oligo(ethylene glycol) monomethyl ether methacrylate (OEOMA) with M = 475 g/mol and pendent EO units DP ≈ 7 from Aldrich was purified by passing it through a column filled with basic alumina to remove the inhibitors.

3.2.4 Synthesis of ss(PLA-OH)$_2$ by ROP

ROP of LA was conducted in the presence of ssDOH difunctional initiator in toluene at 120 °C. The detailed procedure is as follows; ssDOH (45.9 mg, 0.3 mmol), LA (3.0 g, 20.8 mmol), Sn(Oct)$_2$ (6.0 mg, 0.02 mmol), and toluene (2 mL) were added to a 10 mL Schlenk flask. The resulting mixture was deoxygenated by four freeze-pump-thaw cycles. The reaction flask was filled with nitrogen, thawed, and then immersed in an oil bath preheated at 120 °C to start the

polymerization. After 2.5 hrs, the polymerization was stopped and cooled to room temperature. The resulting homopolymers were precipitated from MeOH containing a trace amount of HCl (note that LA is soluble in MeOH). They were then isolated by vacuum filtration and further dried in a vacuum oven at 50 °C overnight, resulting in a white solid.

3.2.5 Esterification to ss(PLA-Br)$_2$

The purified, dried ss(PLA-OH)$_2$ homopolymers were brominated by reacting with Br-iBuBr (10 mole equivalents to hydroxyl groups of ss(PLA-OH)$_2$) in the presence of Et_3N. For the detailed procedure, ss(PLA-OH)$_2$ (4.0 g, 0.6 mmol) and Et_3N (0.6 g, 6.0 mmol) were dissolved in tetrahydrofuran (THF, 50 mL). The resulting mixture was purged with N_2 for 30 min. Br-iBuBr (1.4 g, 6.0 mmol) was added drop-wise for 15 min in an ice bath at 0 °C and then kept at room temperature for 12 hrs. The formed solids (HCl:Et_3N adducts) were removed by a vacuum filtration and then purified by precipitation from MeOH to remove excess Et_3N and Br-iBuBr, which is soluble in MeOH, for the former, or react with MeOH, for the latter. The precipitates were collected and dried in a vacuum oven at room temperature for 12 hrs. The extent of esterification was determined by ^{1}H-NMR in $CDCl_3$.

3.2.6 Synthesis of ssABP-1 by ATRP

The standard procedure for normal ATRP of OEOMA was catalyzed with CuBr/PMDETA in the presence of ss(PLA-Br)$_2$ macro-initiator in THF at 47 °C. The dried, purified ss(PLA-Br)$_2$ (1.0 g, 0.15 mmol), OEOMA (1.4 g, 3.0 mmol), PMDETA (31.5 μL, 0.15 mmol), and THF (3 mL) were mixed in a 10 mL Schlenk flask. The resulting mixture was deoxygenated by four freeze-pump-thaw cycles. The reaction flask was filled with nitrogen and CuBr (21.6 mg, 0.15 mmol) was then added to the frozen solution. The flask was sealed, purged with

vacuum and backfilled with nitrogen once. The mixture was thawed and the flask was then immersed in an oil bath preheated to 47 °C to start the polymerization. Aliquots were withdrawn at different time intervals during the polymerization to monitor conversion and molecular weight by GPC. The polymerization was stopped at 2 hrs by exposing the reaction mixture to air.

The resulting polymers were purified by the removal of residual copper species and unreacted monomers as follows; As-prepared green polymer solutions (ca. 5.5 g) were added drop-wise into hexane (350 mL) under stirring. The green precipitated polymers were passed through a column filled with basic aluminum oxide with THF as an eluent to remove copper species three times. Solvent was removed by rotary evaporation and residual solvent was further removed using a vacuum oven at room temperature overnight, yielding ssABP-1. The theoretical molecular weights over conversion were predicted using the equation: $[OEOMA]_0/[ss(PLA\text{-}Br)_2]_0$ x conversion x MW (OEOMA = 475 g/mol) + MW ($ss(PLA\text{-}Br)_2$ determined by ^1H NMR).

3.2.7 Aqueous micellization

An aqueous KH_2PO_4 buffer solution at pH = 7 was added drop-wise into an organic mixture of the purified, dried polymers and THF. The resulting dispersion was stirred for >12 hrs to remove THF through evaporation, yielding colloidally stable micellar dispersions at various concentrations. For the preparation micelles at 0.1 mg/mL, ssABP-1 or HS-ABP (10 mg), THF (3 mL), and water (100 mL) were used.

3.2.8 Determination of critical micellar concentration (CMC) using a NR probe

A stock solution of NR in THF at 1 mg/mL and a stock solution of ssABP-1 in THF at 1 mg/mL were prepared. Water (10 mL) was then added drop-wise

into mixtures consisting of the same amount of the stock solution of NR (0.5 mL, 0.5 mg NR) and various amounts of the stock solution of ssABP-1. The resulting dispersions were stirred for 12 hrs to remove THF, and were then subjected to filtration using 0.45μm PES filters to remove excess NR. A series of NR-loaded micelles at various concentrations of ssABP-1 ranging from 10^{-6} to 0.1 mg/mL were formed. From their fluorescence spectra recorded with λ_{ex} = 480 nm, the fluorescence intensity at maximum λ_{em} = 620 nm was recorded.

3.2.9 Reductive degradation of ss(PLA-OH)$_2$ and ssABP-1 in DMF

For the degradation of ss(PLA-OH)$_2$ precursors in the presence of DTT, a stock solution of DTT in DMF at 100 mg/mL was prepared. ss(PLA-OH)$_2$ (100 mg, 10.7 μmol) was mixed with the stock solution of DTT (82.3 μL, 53.5 μmol) and DMF (5 mL) under stirring. For ssABP-1 in the presence of DTT, ssABP-1 (50 mg, 3.9 μmol) was mixed with the stock solution of DTT (100 mg/mL, 30.1 μL, 19.5 μmol,) and DMF (5 mL) under stirring. Aliquots of the sample were taken periodically for GPC analysis. For ^{1}H-NMR analysis in $CDCl_3$, DMF was evaporated using a rotary evaporator.

Upon the cleavage of disulfides in ss(PLA-OH)$_2$ in response to DTT, a NMR peak at 2.9 ppm corresponding to methylene protons adjacent to disuflide disappeared and a new peak at 2.75 ppm appeared. This peak can be assigned to methylene protons adjacent to terminal thiol (-SH). In addition, a multiple peak at 4.3-4.5 ppm was split into two distinct peaks: one corresponding to methine protons at the end of chains of PLA block and the other corresponding to methylene protons adjacent to ester linkage.

3.2.10 Thiol-responsive degradation of aqueous micelles

A micellar dispersion of ssABP-1 at 0.1 mg/mL (4 mL, 0.4 mg ssABP-1) was mixed with a stock solution of DTT in water (1 mg/mL, 4.8 μL, 0.03 μmol). DLS was used to measure micellar sizes and size distributions. For GPC measurements, water was evaporated using rotary evaporator and the dried polymer was dissolved in THF.

3.2.11 Encapsulation of Dox

A Dox-loaded micellar dispersion was prepared as follows; an aliquot of ssABP-1 (20 mg), Dox (2.0 mg, 3.45 μmol), and triethylamine (0.47 mg, 4.69 μmol), and DMF (1.9 g) were mixed with water (6 mL) for 2 hrs. The resulting dispersion was dialyzed using a dialysis tubing with MWCO = 3,500 g/mol over water for 24 hrs to remove free Dox. To determine the loading level of Dox by UV/Vis spectroscopy, an aliquot of Dox-loaded micellar dispersion (1 mL) was mixed with DMF (5 mL) to form a clear solution of DMF/water = 5/1 v/v. The UV/Vis spectrum was recorded and the loading level of DOX was calculated by the weight ratio of loaded DOX to dried polymers.

3.2.12 Release of Dox from Dox-loaded micelles upon thiol-responsive degradation

Aliquots of the Dox-loaded micellar dispersion at 1.1 mg/mL (5 mL) was transferred into dialysis tubing and immersed in PBS containing 10 mM GSH at pH = 7.4 (60 mL) as well as PBS (pH = 7.4) as a control; to note the pH was adjusted to 7.4 for the 10mM GSH solution by adding 0.1 M NaOH. The fluorescence spectra of the outer water were measured over 27 hrs. To quantify the % Dox released from micelles, Dox (0.066 mg, equivalent to Dox

encapsulated in 5 mL of Dox-loaded micelles) and Et_3N (0.03 mg, 3 mol equivalents) were dissolved in PBS (60 mL) to measure the fluorescence spectrum.

3.3 Results and discussion

3.3.1 Synthesis of ssABP-1 from a combination of ROP and ATRP

The synthetic strategy to prepare well-controlled PLA-based monocleavable amphiphilic triblock copolymer based on three synthetic steps consists of 1) ROP of LA in the presence of tin octoate ($Sn(Oct)_2$) as a catalyst and 2-hydroxyethyl disulfide (SS-DOH) as an initiator to synthesize ss(PLA-$OH)_2$, 2) esterification of ss(PLA-$OH)_2$ to afford ss(PLA-$Br)_2$ ATRP macro-initiator, and 3) chain extension of ss(PLA-$Br)_2$ with water-soluble POEOMA by ATRP.

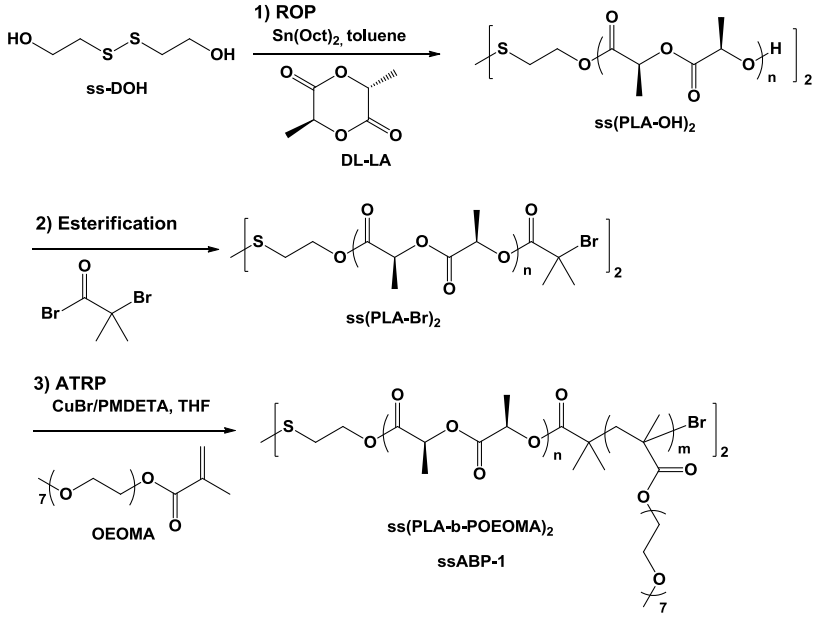

Figure 3.1. Synthetic strategy for the preparation of PLA-based monocleavable triblock copolymers.

As the first synthetic step, well-controlled ss(PLA-OH)$_2$ was synthesized by ROP of LA initiated with ssDOH in the presence of Sn(Oct)$_2$ in toluene at 120 °C (note that D,L-lactide is used in this research). As discussed in section 2.2.1, the ROP of cyclic esters such as LA in the presence of Sn(Oct)$_2$ proceeds via monomer insertion into tin(II)-oxygen bond of alkoxide active centers.[55, 57] As a consequence, the amount of Sn(Oct)$_2$ is an important parameter that influences the rate of ROP. In the experiments, the mole ratio of $[Sn(Oct)_2]_0/[ss\text{-}DOH]_0 = 0.05/1$ was used with $[LA]_0/[ss\text{-}DOH]_0 = 70/1$. The resulting polymers were purified by precipitation from MeOH containing a trace amount of HCl, and then isolated by vacuum filtration. For the purified, dried ss(PLA-OH)$_2$, GPC results indicate molecular weight M_n = 11,000 g/mol with monomodal and narrow molecular weight distribution as low as $M_w/M_n = 1.15$ (Figure 3.2a). Its ^{1}H-NMR spectrum exhibits a triplet (d) at 2.9 ppm corresponding to methylene protons adjacent to disulfides and a multiplet (b) at 5.1-5.3 ppm corresponding to methine protons in PLA blocks (Figure 3.2b). From the integral ratio [(b/2)/(d/2)], the DP of ss(PLA-OH)$_2$ was determined to be 65, corresponding to theoretically calculated $M_{n,theo}$ = 9,400 g/mol. Note that the molecular weight determined by GPC which was calibrated with polystyrene standards is larger than the theoretically estimated one; the difference is attributed to the different hydrodynamic volume of ss(PLA-OH)$_2$ from PSt homopolymers in THF.

Next, well-defined ss(PLA-OH)$_2$ was converted to ss(PLA-Br)$_2$ functionalized with terminal bromine groups by reacting with Br-iBuBr at ambient temperature. ^{1}H-NMR results show the disappearance of peaks at 4.3-4.4 ppm (c) corresponding to terminal methine protons of ss(PLA-OH)$_2$ and the appearance of two new peaks at 1.95 ppm (f) corresponding to six methyl protons adjacent to bromine. The integral ratio of peaks [(f/6)/(d/2)] suggests >95% functionalizaton of ss(PLA-OH)$_2$ with bromines to ss(PLA-Br)$_2$ (Figure 3.2a).

The purified ss(PLA-Br)$_2$ was used as a macroiniator for ATRP of OEOMA under the following conditions: mole ratio of [OEOMA]$_0$/[ss(PLA-Br)$_2$]$_0$/[CuBr/PMDETA]$_0$ = 20/1/0.5 in THF at 45 °C. The polymerization was well-controlled due to the following characteristics: first-order kinetics, linear increase of molecular weight with conversion, and narrow molecular weight distribution (Figure A.1). After the polymerization was stopped at 2 hrs, the resulting triblock copolymers were purified by removal of Cu species and unreacted monomers. GPC results show the evolution of GPC trace to high molecular weight region with no significant traces of ss(PLA-Br)$_2$ macro-initiator remaining and M_n = 15,600 g/mol with M_w/M_n = 1.13 (Figure 3.2b). ^{1}H NMR analysis by taking the integral ratio of peaks [(g/3)/(b/2)] with the DP of PLA block = 65 allows to determine the DP = 13 of the POEOMA blocks (Figure 3.2a). These results suggest the synthesis of well-controlled ss(PLA$_{32}$-b-POEOMA$_7$)$_2$ triblock copolymer.

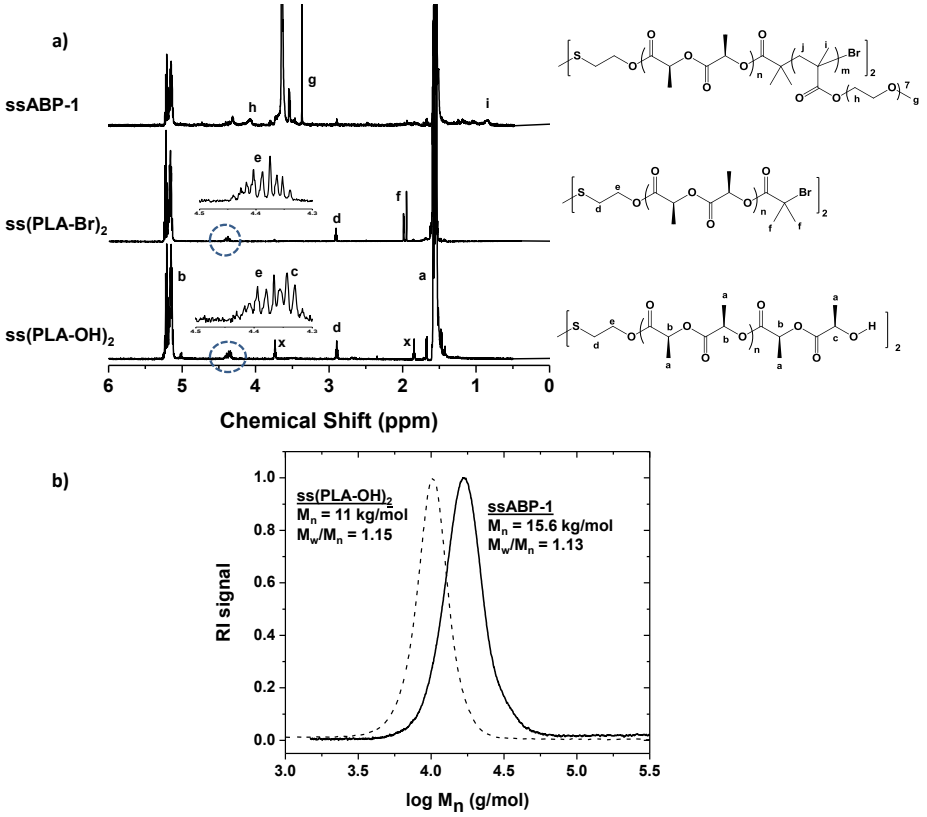

Figure 3.2. ^{1}H-NMR spectra of ss(PLA-OH)$_2$, ss(PLA-Br)$_2$, and ssABP-1 in $CDCl_3$ where x denotes a trace of THF (a), GPC traces of ssABP-1 compared with ss(PLA-OH)$_2$ precursor (b).

3.3.2 Aqueous micellization of ssABP-1

Due to the amphiphilic nature of the ssABP-1, the triblock copolymers were allowed to self-assembe using the solvent-evaporation technique discussed in section 2.3.1 to form micellar aggregates consisting of disulfide-labeled PLA cores surrounded with POEOMA coronas. First, the CMC was determined using fluorescence spectroscopy with a Nile Red (NR) probe.[27b, 74] For the experiment, a series of mixtures consisting of the same amount of NR and varying amounts of

ssABP-1 ranging from 10^{-6} to 0.1 mg/mL in aqueous solution were prepared by the solvent evaporation technique where THF was removed by evaporation and free NR by filtration. Figure 3.3a shows that the fluorescence intensity was significantly low and did not change for lower concentrations. However, it increased with an increasing concentration of ssABP-1. From two equations obtained by fitting each data set to a linear relationship, the CMC of ssABP-1 was determined to be 5 μg/mL. Then, micelles were prepared using the same solvent-evaporation technique at a concentration of 0.1 mg/mL and their size was characterized by DLS. Results show a monomodal distribution with an average diameter of 80 nm (Figure 3.3b).

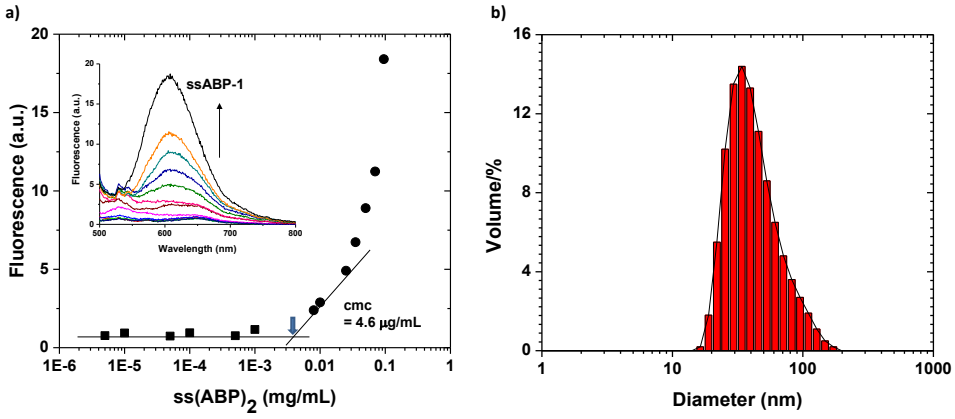

Figure 3.3. Fluorescence intensity of Nile Red for aqueous mixtures consisting of NR with various amounts of ssABP-1 to determine the CMC (a), DLS diagram of ssABP-1 micelles at a concentration of 0.1 mg/mL in deionized water (b).

3.3.3 Reduction-responsive disulfide bond cleavage

Thiol-responsive degradation and the concomittant morphological variance was investigated for both the polymer chains and micellar systems. In the first step, several aspects of the thiol-responsive degradation was examined; ss(PLA-OH)$_2$ precursors and ssABP-1 were dissolved homogenesouly in DMF

and their degradation was examined. It is reported that the degradation is enhanced with an increasing amount of thiols.[35c, 75] For this experiment, an aliquot of the purified, dried ss(PLA-OH)$_2$ with DP = 65 was mixed with DTT (5 mole equivalent to disulfides). ^{1}H-NMR results suggest the significant cleavage of disulfide linkages in ss(PLA-OH)$_2$, yielding HS-PLA-OH as a cleaved product (see ^{1}H-NMR spectra of ss(PLA-OH)$_2$ before and after the cleavage of disulfides in Figure A.2). GPC traces became bimodal with the occurrence of a new peak in low molecular weight region (Figure 3.4a). With an increasing degradation time, the new peak corresponding to HS-PLA-OH increased, while the original peak corresponding to ss(PLA-OH)$_2$ decreased. Peak analysis results suggest that the degradation of ss(PLA-OH)$_2$ upon the cleavage of disulfide linkages increased over time, reaching >80% in 8 hrs. Molecular weight also decreased from M_n = 11,000 g/mol to M_n = 7,000 g/mol. Such decrease is attributed to the cleavage of disulfide linkages in response to DTT. In order to examine the effect of chain length of ss(PLA-OH)$_2$ on the cleavage rate of disulfide linkages, another sample of ss(PLA-OH)$_2$ with DP = 46 was synthesized and then mixed with DTT (5 mole equivalent to disulfides) in DMF under similar conditions. GPC results indicate that the molecular weight rapidly decreased from M_n = 9,600 g/mol to M_n = 5,000 g/mol within 2 hrs. These results suggest an enhanced degradation of ss(PLA-OH)$_2$ with a decreasing chain length. Next, an aliquot of ssABP-1 triblock copolymers was mixed with 5 mole equivalent DTT to disulfides in DMF. GPC results indicate that its molecular weight decreased from M_n = 15,800 to 9,500 g/mol over 30 hrs at room temperature (Figure 3.4b). Compared to ss(PLA-OH)$_2$, the slow degradation of ssABP-1 is probably attributed to both larger chain length and presence of bulky POEOMA block.

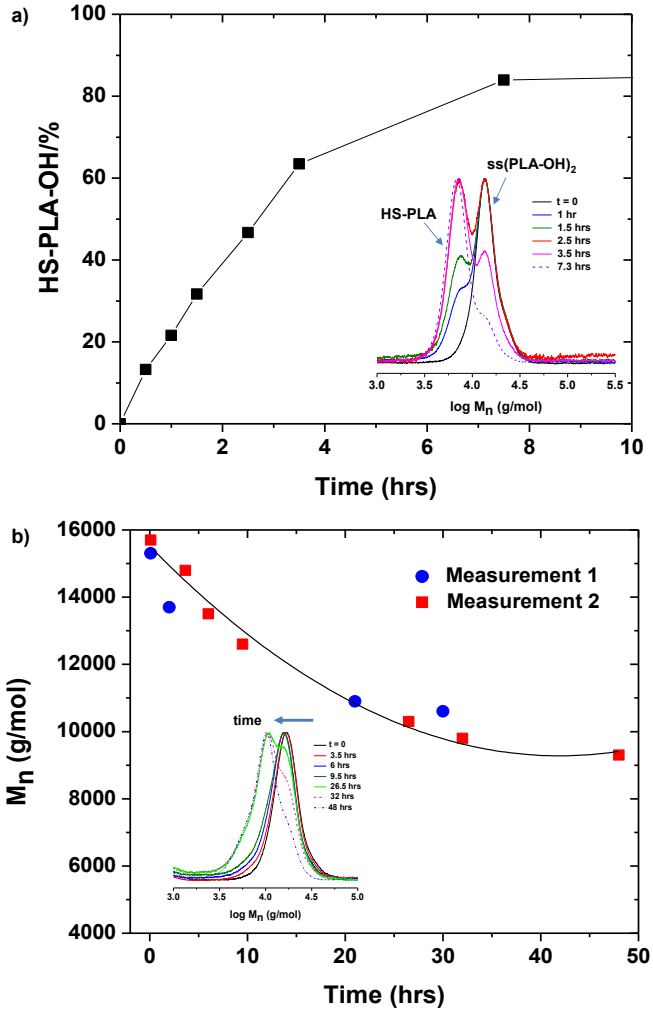

Figure 3.4. GPC results for the degradation of ss(PLA-OH)$_2$ (a) and ssABP-1 (b) mixed with 5 mole equivalent DTT to disulfides in DMF.

In the subsequent step, the thiol-induced degradation of the micelles was studied using DLS. Here, a micellar dispersion of ssABP-1 at 0.1 mg/mL was mixed with a stock solution of DTT in water and the changes in size were followed using DLS. DLS results indicate that their diameter slightly decreased from 80 to 74 nm in the presence of DTT after 2 days (Figure 3.5a and b). After

water was removed, the degraded polymers had a M_n = 8,400 g/mol (Figure 3.5c). These results suggest that the central single disulfide linkage of ssABP-1 in the micellar core is cleaved in response to thiols yielding amphiphilic HS-PLA-b-POEOMA (HS-ABP). For other mono-cleavable micelles of triblock copolymers having single disulfide, the significant changes in their sizes due to destabilization upon the cleavage of disulfide linkages are reported.[36a, 37] The difference in destabilization of mono-cleavable micelles is due to the nature and chain length of hydrophobic and hydrophilic blocks.[39b]

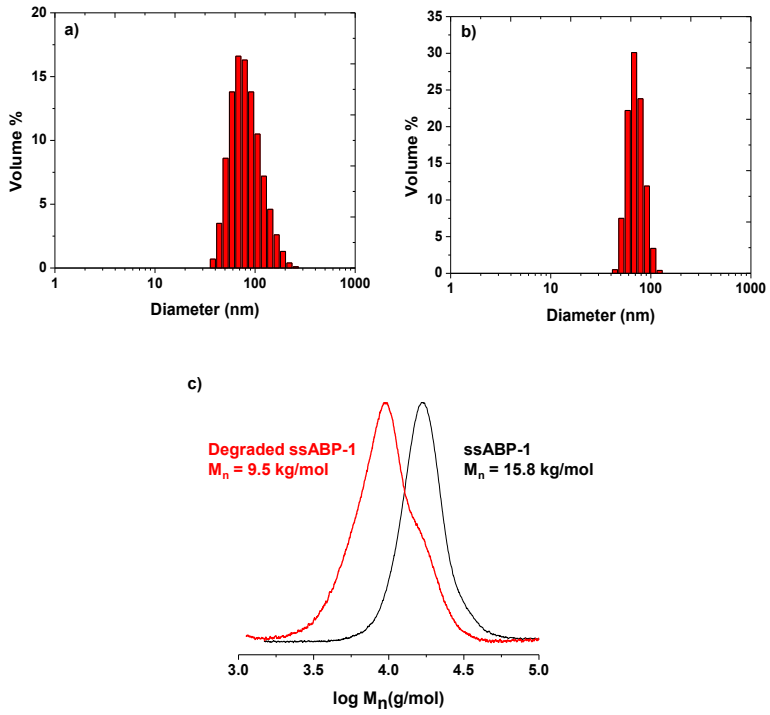

Figure 3.5. DLS diagram of ssABP-1-based micelles before (a) and 2 days after (b) the addition of DTT and GPC traces of ssABP-1 micelles without and with 10 mM DTT after removal of water (c).

3.3.4 Thiol-triggered drug release from Dox-loaded ssABP-1

Finally, the thiol-triggered drug release of encapsulated anticancer drugs, here doxorubicin (Dox), from Dox-loaded micellar aggregates was investigated. Dox-loaded micellar aggregates at 1.1 mg/mL were prepared using a dialysis method. Using the absorbance at λ_{max} = 497 nm (Figure A.3) and the pre-determined extinction coefficient, ε = 12,400 $M^{-1}cm^{-1}$ in a mixture of DMF/water = 5/1 v/v,[53] the loading level of Dox was determined to be 1.2%. To examine the release of encapsulated Dox in response to GSH, aliquots of the dispersion was placed in a dialysis tubing with MWCO = 3,500 g/mol and was dialyzed over a PBS solution of 10 mM GSH. The results were compared with a control (dialysis without GSH). Note that the PBS solutions were adjusted to pH 7.4 with the addition of 0.1 M NaOH in order to eliminate concerns about the enhanced degradation of PLA in acidic pH. The reductive release of Dox from micelles was followed using fluorescence spectroscopy. The fluorescence intensity (FI) of Dox measured at λ_{max} = 590 nm, which corresponds to Dox released from Dox-loaded micelles, was recorded in the outer solution at given time intervals. Figure A.4 shows the evolution of fluorescence spectra of outer water (λ_{ex} = 470 nm) over time and % Dox release over time is constructed in Figure 3.6. As can be seen, in the presence of 10 mM GSH, the release of Dox was enhanced, compared to without GSH, as a result of thiol-induced degradation of micelles by cleavage of disulfides.

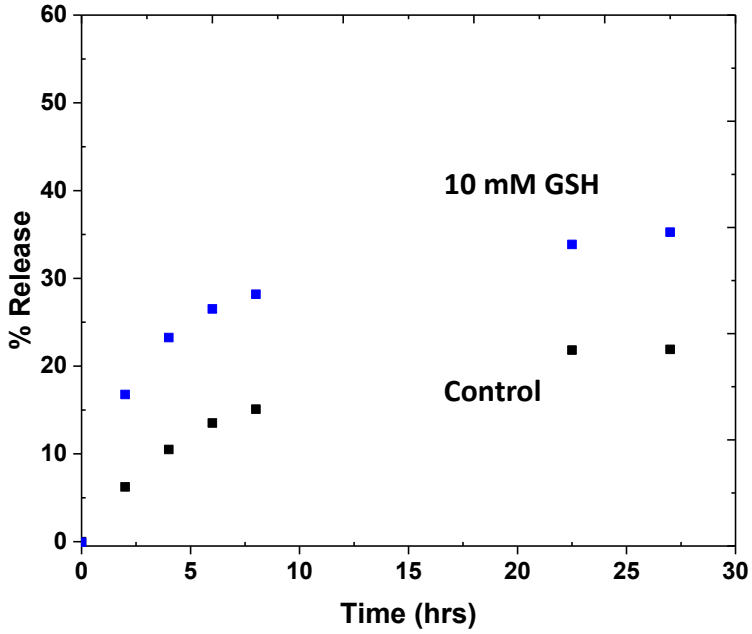

Figure 3.6. % release profiles of Dox from Dox-loaded micelles in the absence (control) and presence of 10 mM GSH in PBS solution adjusted to pH = 7.4.

3.4 Conclusion

New thiol-responsive degradable PLA-based micelles having disulfide linkages in the middle of triblock copolymers (ssABP-1) were prepared by a combination of ROP in the presence of a disulfide-labeled diol as an initiator and ATRP. GPC and NMR results suggest that both polymerizations proceeded in a living manner, allowing for the synthesis of well-defined ss(PLA-OH)$_2$ and ssABP-1 with monomodal and narrow molecular weight distribution with M_w/M_n < 1.15. Aqueous micellization of these ssABP-1 formed self-assembled micellar aggregates with disulfide-containing PLA cores. Because of the presence of central disulfides, these polymers were degraded in response to thiols upon the cleavage of the disulfide linkage. Such thiol-triggered degradation resulted in enhanced release of encapsulated anticancer drug to some extent.

Chapter 4

Alternative method to synthesize reduction-responsive PLA-based monocleavable micelles

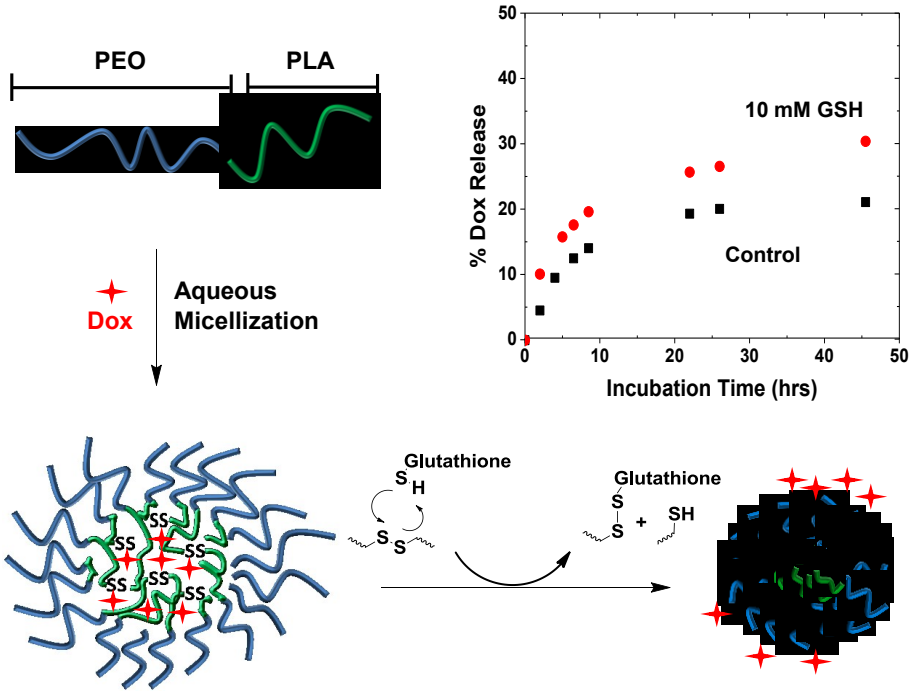

A new approach utilizing a combination of ring-opening polymerization and facile coupling reactions is explored to synthesize a reduction-responsive triblock copolymer comprising biocompatible PLA block and poly(ethylene oxide) (PEO) block, thus the formation of ss(PLA-b-PEO)$_2$ ssABP-2. This

copolymer self-assembles to form colloidally-stable mono-cleavable micelles having single disulfides in hydrophobic PLA cores surrounded with PEO coronas in aqueous solution. The reductive cleavage of the core disulfides results in changes in micellar sizes, depending on the size and nature of reducing agents. The size increases in the presence of glutathione (a cellular reducing agent), which enhances the release of encapsulated anticancer drugs *in vitro*. For biological prespectives, the ssABP-2 micelles having hydrophilic PEO corona exhibit enhanced colloidal stability with no significant non-specific interactions with proteins.

This chapter contains information that was published in *Colloids and surfaces B: Biointerfaces*, **2014**, *In press, DOI: 10.1016/j.colsurfb.2014.08.002* and part of the chapter is reproduced from the article with permission from the publisher.

4.1 Introduction

Well-defined block copolymers exhibiting stimuli-responsive degradation (SRD) have attracted significant attention in constructing novel nanomaterials;[28, 76] typical examples include tunable thermoresponsive polymers,[77] nanoporous films,[78] nanofibers,[79] crosslinked nanogels,[80] and self-assembled micelles.[32, 81] These SRD block copolymers are generally designed to have dynamic covalent bonds (i.e. cleavable linkages), which are later cleaved in response to external stimuli. The reduction-responsive disulfide linkages are of particular interest. Disulfides are cleaved to the corresponding thiols in the presence of a thiol reducing agent.

A number of disulfide-containing block copolymers and their self-assembled nanostructures have been developed.[73a, 82] These block copolymers are designed with varying numbers of disulfides positioned in single locations, including at block junctions[33b, 33e, 33i, 33j, 35c] and as crosslinks[83] as well as in pendant chains[34a, 34c-e] and main chains.[35a, 35c, 35d, 84] An interesting system contains a disulfide linkage in the center of a triblock copolymer (i.e. AB-SS-BA, A and B denoted as a block) which self-assembles to form monocleavable micelles having disulfide linkages in the hydrophobic cores.[85] Upon cleavage of the disulfide linkages in response to reductive reactions, the cleaved copolymers with shorter chain lengths remain amphiphilic (i.e. HS-BA) in micellar forms. Such a process produces a change in size and morphology in the monocleavable micelles. However, a limited number of reports describe the methods to synthesize monocleavable AB-SS-AB copolymers and their self-assembled micelles. For example, a thiol-alkyne click[37] reaction and ROP[38] were used to synthesize branched copolymers, while reversible addition-fragmentation chain transfer (RAFT) polymerization[39] and atom-transfer radical polymerization

(ATRP), as presented in the previous chapter, were explored to synthesize linear diblock copolymers.

The purpose of the research presented in this chapter was to explore a new strategy to synthesize monocleavable micelles consisting of hydrophobic PLA and hydrophilic PEO (Figure 4.1). PLA is biocompatible, FDA-approved for clinical use, and biodegradable through enzymatic reactions and hydrolysis in physiological conditions.[9, 41, 55] The present strategy is based on utilizing PEO because it is biocompatible and also FDA-approved for clinical use as well as defined by low toxicity.[86] Furthermore, PEO prevents nonspecific protein adsorption, thus prolonging blood circulation for PLA-based nanocarriers.[48, 87] The new strategy is centered on a facile carbodiimide coupling reaction between PEO and PLA having a disulfide in the middle, thus PEO-b-PLA-SS-PLA-b-PEO ssABP-2. The resulting ssABP-2 copolymers and their self-assembled micelles were characterized for reduction-responsive degradation and release of encapsulated anti-cancer drugs, as well as non-specific protein adsorption.

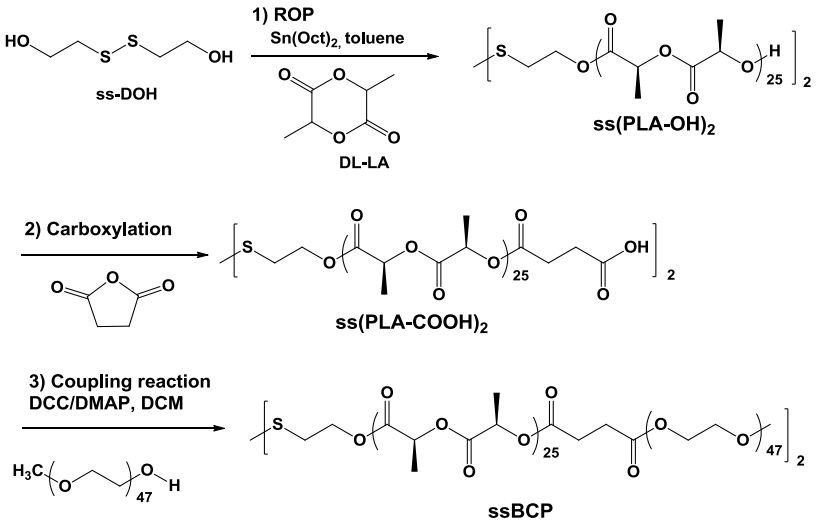

Figure 4.1. Synthetic strategy for the preparation of well-controlled reduction-responsive ssABP-2 triblock copolymers.

4.2 Experimental

4.2.1 Instrumentation and analyses

The details are described in section 3.2.1 of chapter 3 (page 33).

4.2.2 Transmission Electron Microscope (TEM) images

TEM images were obtained using a Philips Tecnai 12 TEM, operated at 120 kV and equipped with a thermionic LaB6 filament. An AMT V601 DVC camera with point to point resolution and line resolution of 0.34 nm and 0.20 nm respectively was used to capture images at 2048 by 2048 pixels. The specimen preparation was carried out as follows, a micellar dispersion was dropped onto a copper TEM grid (400 mesh, carbon coated), blotted and allowed to dry at room temperature.

4.2.3 Materials

Poly(ethylene oxide) methyl ether (PEO) (MW = 2,000 g/mol), 2-hydroxyethyl disulfide (ssDOH), 3,6-dimethyl-1,4-dioxane-2,5-dione (DL-lactide, LA), tin(II) 2-ethylhexanoate ($Sn(Oct)_2$, 95%), succinic anhydride (SA), triethylamine (Et_3N), 4-(dimethylamino)pyridine (DMAP), N,N′-dicyclohexylcarbodiimide (DCC), Nile Red (NR), L-glutathione reduced (GSH) and doxorubicin hydrochloride (DOX, $-NH_3^+Cl^-$ forms, > 98%) from Aldrich; DL-dithiothreitol (DTT, 99%) from Acros Organics; and Bovine Serum Albumin (BSA, > 95%) from MP biomedicals were purchased and used as received. Dialysis tubing with MWCO = 12,000 Da was purchased from Spectrum Labs.

4.2.4 Synthesis of $ss(PLA\text{-}OH)_2$ by ROP

The details are described in section 3.2.4 of chapter 3 (pages 35-36).

4.2.5 Carboxylation of ss(PLA-OH)$_2$ to ss(PLA-COOH)$_2$

The purified, dried ssPLA-OH homopolymers were carboxylated by reacting with succinic anhydride (50 mole equivalents to hydroxyl groups of ss(PLA-OH)$_2$) in the presence of Et_3N. The purified, dried ss(PLA-OH)$_2$ (2.4 g, 0.25 mmol), succinic anhydride (1.23 g, 12.3 mmol), and DMAP (15 mg, 0.12 mmol) were dissolved in tetrahydrofuran (THF, 20 mL). The resulting mixture was purged with N_2 for 30 min. Et_3N (1.24 g, 12.3 mmol) was added drop-wise for 15 min and kept at room temperature for 12 hrs. The resulting mixture was concentrated by evaporating THF and precipitated from aqueous HCl solution to remove excess Et_3N and unreacted succinic anhydride. The precipitates were dissolved in THF and the precipitation procedure was repeated three times. The resulting ss(PLA-COOH)$_2$ precipitates were dried in a vacuum oven at room temperature for 12 hrs.

4.2.6 Synthesis of ssABP-2 by DCC coupling

A solution of DCC (0.15 g, 0.70 mmol) in DCM (4 mL) was added drop-wise to a solution containing ss(PLA-COOH)$_2$ (1.72 g, 0.18 mmol), PEO (0.70 g, 0.35 mmol), and DMAP (2 mg, 0.018 mmol) in DCM (30 mL) while stirring in an ice-bath at 0 °C for 20 min under nitrogen atmosphere. The resulting mixture was allowed to stir at room temperature for 12 hrs. The dicyclohexylurea (DCU) formed as a byproduct was removed by vacuum filtration and DCM was removed by evaporation.

For purification, the residues were dissolved in DMF and dialyzed in deionized water for 2 days to remove residual PEO and other starting materials. Afterwards, water was removed by rotary evaporation, the polymeric residues dissolved in THF, and precipitated from cold MeOH. The residual ss(PLA-COOH)$_2$ as precipitates were removed by vacuum filtration. The supernatant was

evaporated by rotary evaporation, and the remaining residues were dried in a vacuum oven at room temperature for 12hrs to yield ssABP-2.

4.2.7 Determination of critical micellar concentration (CMC) using a NR probe

The details are described in section 3.2.8 of chapter 3 (pages 37-38).

4.2.8 Aqueous self-assembly

Deionized water was added drop-wise into organic solutions consisting of the purified, dried ssABP-2 dissolved in THF. The resulting dispersions were stirred for >12 hrs to remove THF, yielding colloidally stable micellar dispersions at various concentrations. For the preparation of micelles at 1 mg/mL, ssABP-2 or HS-ABP (10 mg), THF (3 mL), and water (10 mL) were used.

4.2.9 Reductive cleavage of disulfide linkages in ssABP-2

Aliquots of the purified, dried ssABP-2 (100 mg, 8.0 μmol disulfides) were mixed with DTT (100 mg/mL, 77 μL, 50 μmol) in DMF (5 mL) under stirring. Aliquots of the sample were taken periodically for GPC analysis. Upon the complete degradation of ssABP-2, the degraded polymer solution in DMF was dialyzed in deionized water to remove excess DTT and DMF. Then, the resulting aqueous dispersion was analyzed by DLS.

4.2.10 Reduction-responsive degradation of ssABP-2 micelles

Aliquots of ssABP-2 micelle dispersions at 5.8 mg/mL (8.6 mL) were mixed with a stock solution of DTT in water (1 mg/mL, 132 μL, 86 μmol). In addition, aliquots of ssABP-2 micelle dispersion at 1.3 mg/mL were mixed with a stock solution of GSH in water (1mg/mL, 222 μL, 72 μmol). DLS was used to follow

changes in micelle size and size distribution. For GPC measurements, water was evaporated using rotary evaporation and the dried polymer was dissolved in THF.

4.2.11 Encapsulation of Dox

Clear solutions consisting of an aliquot of ssABP-2 (20 mg), Dox (2.0 mg, 3.45 μmol), Et_3N (1.05 mg, 10.38 μmol), and DMF (3 mL) were mixed with water (10 mL) and stirred for 2 hrs. The resulting dispersion was dialyzed in deionize water (1L) over 24 hrs to form Dox-loaded micelle dispersion at 1.1 mg/mL. To determine the loading level of Dox by UV/Vis spectroscopy, an aliquot of Dox-loaded micellar dispersion (1 mL) was mixed with DMF (5 mL) to form a clear solution of DMF/water = 5/1 v/v. The UV/Vis spectrum was recorded and the loading level of DOX was calculated by the weight ratio of loaded DOX to dried polymers.

4.2.12 GSH-triggered Dox release from Dox-loaded micelles

Aliquots of the Dox-loaded micellar dispersion at 1.1 mg/mL (5 mL) was transferred into dialysis tubing immersed in PBS containing 10 mM GSH at pH = 7.4 (60 mL) as well as PBS (pH = 7.4) as a control. The fluorescence spectra of the outer water were measured over 46 hrs. To quantify the %Dox released from micelles, Dox (0.12 mg, equivalent to Dox encapsulated in 5 mL of Dox-loaded micelles) and Et_3N (0.06 mg, 3 mol equivalents) were dissolved in PBS (60 mL) to measure the fluorescence spectrum.

4.2.13 Non-specific interaction of ssABP-2 micelles with BSA

A similar procedure for the aqueous self-assembly described above was used to prepare a micellar dispersion of ssABP-2 at 13 mg/mL. Then, an aliquot (1 mL) was mixed with two different volumes (1 mL and 2 mL) of an aqueous

BSA solution in PBS (13 mg/mL). DLS was used to follow any changes in micelle size and size distribution.

4.3 Results and discussion

4.3.1 Synthesis of ssABP-2

As illustrated in Figure 4.1, the approach for the synthesis of ssABP-2 (i.e. PEO-b-PLA-ss-PLA-b-PEO) triblock copolymers having disulfides in the middle of central PLA block consists of three steps. The first step is the synthesis of well-controlled ss(PLA-OH)$_2$ by ring opening polymerization of LA in the presence of Sn(Oct)$_2$ in toluene at 120 °C. The polymerization conditions include $[LA]_0/[ssDOH]_0/[Sn(Oct)_2]_0$ = 70/1/0.05 and weight ratio of LA/toluene = 1.5/1. The detailed procedure is described in the previous chapter. The purified ss(PLA-OH)$_2$ had the molecular weight M_n = 9,300 g/mol and M_w/M_n = 1.09 determined by GPC (Figure 4.2) and the degree of polymerization (DP) = 50 determined by ^{1}H-NMR from the integral ratio of peaks (b/d) (Figure 4.3a). The second step consists of the facile coupling of ss(PLA-OH)$_2$ with excess succinic anhydride (SA) in DMF at room temperature. The resulting ss(PLA-COOH)$_2$ was purified by precipitation from water to remove unreacted SA. As seen in Figure 4.3b, a new peak at 2.7 ppm (f) corresponding to eight methylene protons in the SA moiety appeared, while a peak at 4.3 ppm (e) corresponding to two terminal methine protons in ss(PLA-OH)$_2$ disappeared. The integral ratio of peaks (f/d) indicates high carboxylation (>97%).

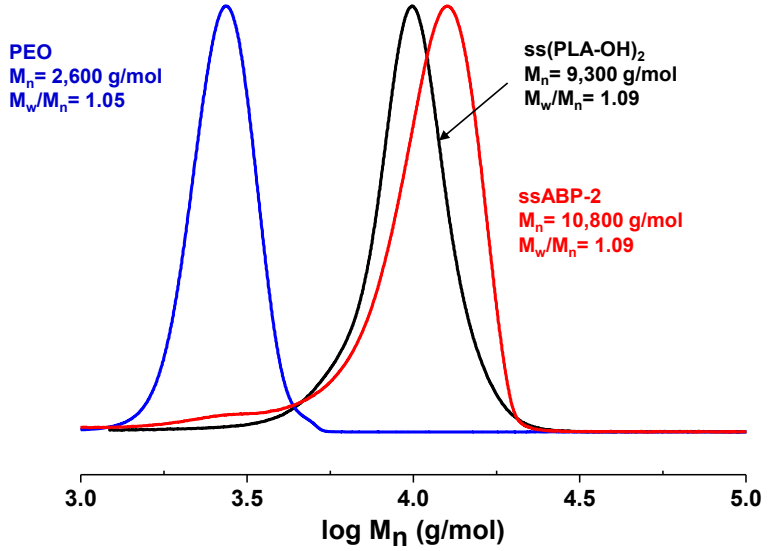

Figure 4.2. GPC traces of ssABP-2, compared with ss(PLA-OH)$_2$ and PEO precursors.

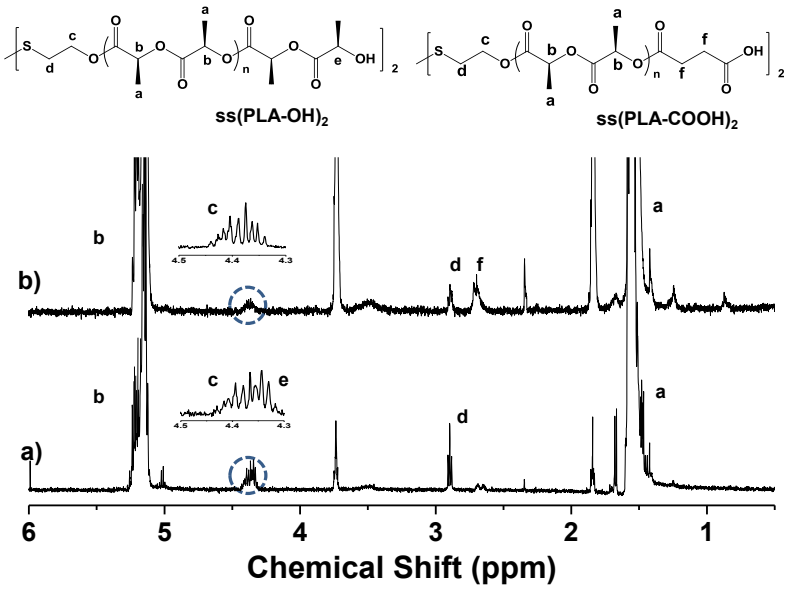

Figure 4.3. ^{1}H-NMR spectra of purified ss(PLA-OH)$_2$ (a) and ss(PLA-COOH)$_2$ (b) in $CDCl_3$.

After the successful synthesis and characterization of ss(PLA-COOH)$_2$ having terminal COOH groups, the third step is a carbodiimide coupling reaction of ss(PLA-COOH)$_2$ with PEO under conditions including the initial mole equivalent ratio of $[OH]_0/[COOH]_0 = 1/1$ in the presence of excess DCC (4 mole equivalent to OH groups) in DCM at 0 °C for 12 hrs. As seen in Figure B.1, the reaction mixture contains ssABP-2 triblock copolymers and also residual PEO and ss(PLA-COOH)$_2$. Thus, the resulting triblock copolymer was purified with multiple steps including 1) removal of dicyclohexyl urea (a byproduct of the DCC coupling reaction) by vacuum filtration and DCM by evaporation; 2) intensive dialysis of the resulting polymeric residues dissolved in DMF over water to remove residual PEO; 3) lyophilation to remove water; 4) precipitation of the residues dissolved in THF from MeOH to remove unreacted ss(PLA-COOH)$_2$ or ssPLA species as precipitates; and 5) further evaporation of MeOH. GPC results of the purified polymers indicate the clean evolution of GPC trace to high molecular weight region, with an increasing M_n = 10,900 g/mol. Furthermore, no significant residues of ss(PLA-COOH)$_2$ and PEO remained which suggests the purification method was efficient (Figure 4.2). ^{1}H-NMR spectrum in Figure 4.4 shows a new triplet at 4.2 ppm corresponding to the four methylene protons adjacent to the ester linkage, confirming the occurrence of coupling reaction between COOH group in ss(PLA-COOH)$_2$ and OH group in PEO. From the integral ratio of (g/f), the coupling efficiency was determined to be >98%. These results suggest the successful synthesis of ssABP-2 (PEO_{47}-b-PLA_{25}-ss-PLA_{25}-b-PEO_{47}).

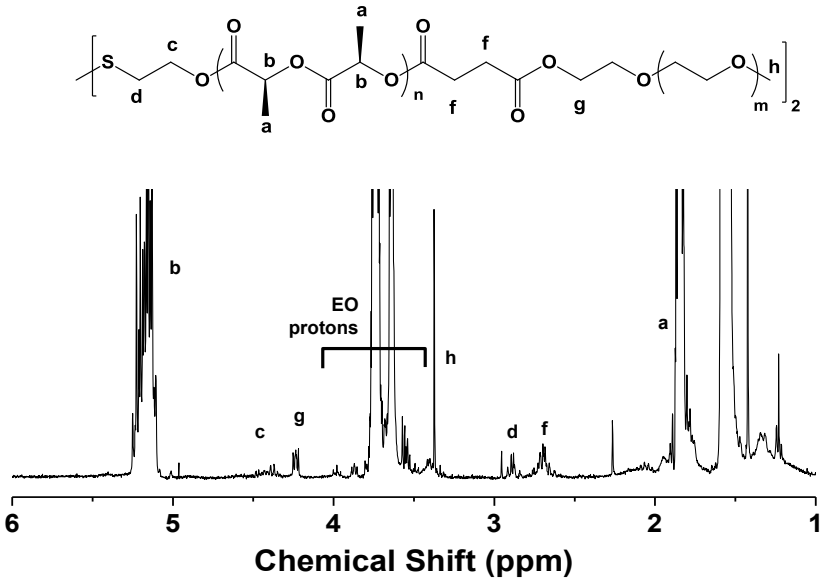

Figure 4.4. ^{1}H-NMR spectrum of ssABP-2 in $CDCl_3$.

4.3.2 Aqueous micellization of ssABP-2

The resulting ssABP-2 triblock copolymer consisting of hydrophilic PEO and hydrophobic PLA-ss-PLA blocks is amphiphilic and may self-assemble in aqueous solution to form micellar aggregates consisting of hydrophobic PLA core surrounded with PEO coronas. First, their critical micellar concentration was determined by fluorescence spectroscopy using a NR probe. As seen in Figure 4.5, the fluorescence (FL) intensity of NR was significantly low and did not change at low concentrations of ssABP-2. This is due to a significant amount of NR molecules remaining in water because the concentration of ssABP-2 is not high enough for the formation of micelles. However, it increased with an increasing concentration of ssABP-2. Such FL increase is attributed to the formation of ssABP-2 micelles that enable the encapsulation of NR molecules in

hydrophobic micellar cores. From two linear regressions, the CMC of ssABP-2 was determined to be 13 μg/mL.

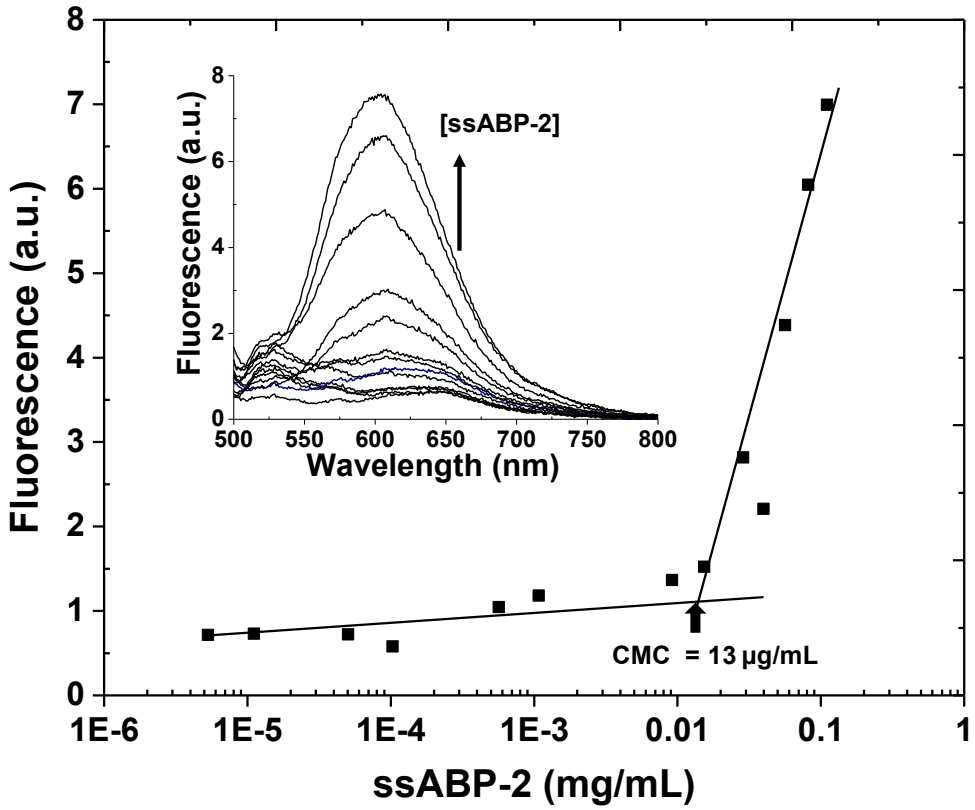

Figure 4.5. Overlaid fluorescence spectra (inset) and fluorescence intensity at λ = 620 nm for aqueous mixtures consisting of NR with various amounts of ssABP-2 to determine the CMC.

Then, aqueous micellization through self-assembly of ssABP-2 was examined at 1.3 mg/mL, above the CMC, using a solvent evaporation method. DLS results of the prepared nanoparticles suggests the formation of colloidally stable micellar aggregates with a diameter of 21 nm (Figure 4.6a). Furthermore, TEM images of the micellar aggregates were obtained to corroborate the DLS results and obtain information with regards to the morphology of the partciles. The TEM images indicate a diameter of 17 nm with a spherical morphology,

which is smaller than that determined by DLS, due to the dehydrated state of the micelles (Figure 4.6b).

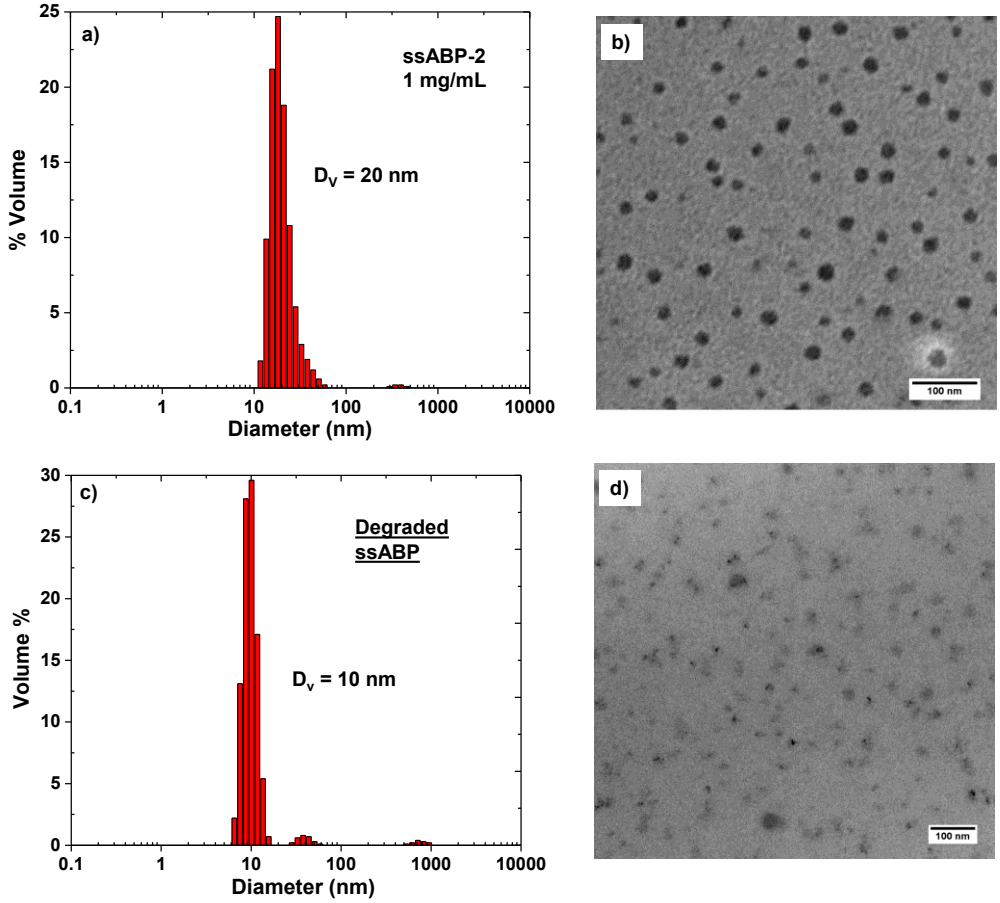

Figure 4.6. DLS diagrams (a, c) and TEM images (b, d) of aqueous micelles before (a, b) and after (c, d) treatment with 10mM DTT in aqueous solution at 1.3 mg/mL.

4.3.3 Thiol-induced degradation of ssABP-2 triblock copolymers

In order to characterize the ssABP-2 system for its propensity towards thiol-triggered drug release, initial studies were performed to determine the response of ssABP-2 triblock copolymer and its self-assembled nanostructures

towards reduction reactions. First, the reductive cleavage of disulfides was examined under homogeneous conditions. Aliquots of the purified ssABP-2 were mixed with DTT in DMF. DTT is commonly used as an amphiphilic reducing agent which is soluble in most common organic solvents including DMF. As seen in Figure 4.7, the molecular weight rapidly decreased from M_n = 10,800 g/mol to M_n = 6,100 g/mol within 1 hr. This decrease in molecular weight results from the cleavage of the disulfide linkages in the middle of the central hydrophobic block. Following thiol-triggered degradation of ssABP-2 triblock copolymers in DMF, the degradation of self-assembled micelles in aqueous solution (heterogeneous conditions) was examined. Two reducing agents including DTT and GSH were examined, since GSH is a cellular trigger. Aliquots of the micellar dispersions were mixed with 10 mM DTT (micelles at 1.3 mg/mL) and 10 mM GSH (micelles at 5.8 mg/mL) at room temperature. The change in size was followed using DLS. When the micelles were treated with DTT, their diameters gradually decreased from 20 nm to 10 nm over a period of 72 hrs (Figure 4.8). Similar decrease in size in the presence of DTT has been reported for other mono-cleavable micelles with different structures of ABPs.[37-38] The degraded products were further analyzed using GPC, after the removal of water, in order to correlate the change in micelle size to a reduction of the disulfide bond. As seen in Figure 4.7, the degraded products in the presence of DTT had decreased molecular weight to M_n = 6,300 g/mol. This value is similar to that (6,100 g/mol) of the degraded products in DMF (homogeneous solution). These results suggest that the decrease in micelle size is a consequence of the cleavage of the central disulfide linkage in response to DTT, yielding degraded PEO-b-PLA-SH. In a control experiment, the degraded products (PEO-b-PLA-SH) in DMF were micellized in order to study their size using DLS and the results show that the cleaved shABP-2 formed smaller-sized nanostructures with a diameter of 10 nm by DLS and 9 nm

by TEM (Figure 4.6c). However, their morphologies were not well-defined, as seen in TEM image (Figure 4.6d).

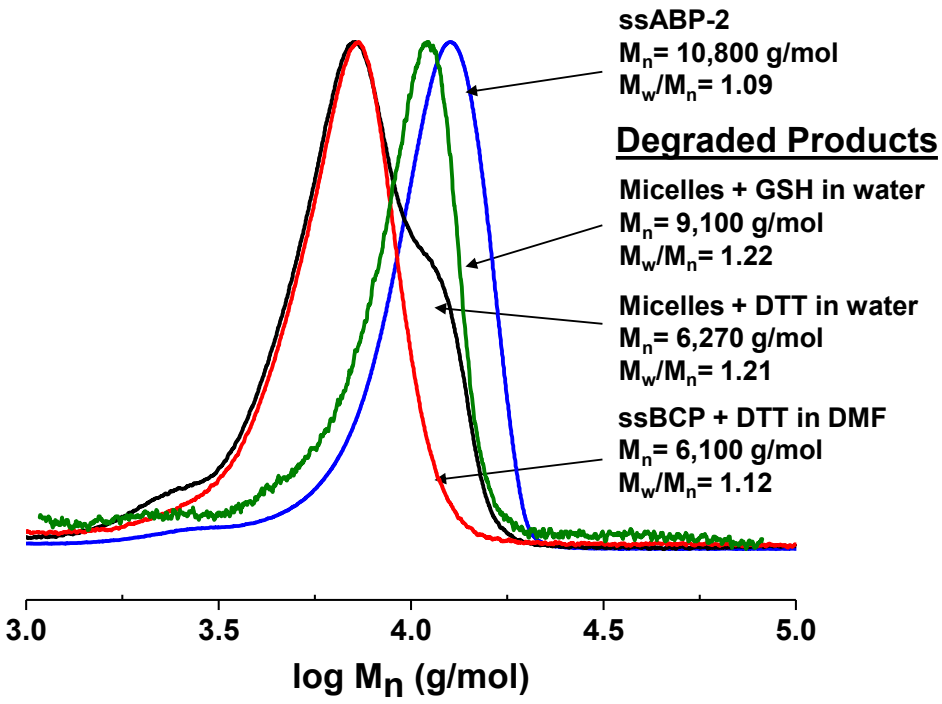

Figure 4.7. GPC traces of ssABP-2 before and after treatment with DTT in DMF as well as ssABP-2 micelles treated with DTT and GSH in water. For micelle sample, water was removed for GPC measurements.

Interestingly, in the presence of GSH (10 mM) the particle size increased with an occurrence of larger aggregates (Figure 4.8), which opposes the size decrease observed for the DTT-treated micelles. GPC analysis of the degraded products in the presence of GSH indicate a decrease in the molecular weight to M_n = 9,100 g/mol which is larger than that for the DTT-treated micelle and the degraded product in DMF. A proposed degraded product in the presence of GSH includes PEO-b-PLA-SS-GSH. The presence of terminal GSH moiety could

explain the larger micelle size and the relatively larger molecular weight of the degraded product in the presence of GSH.

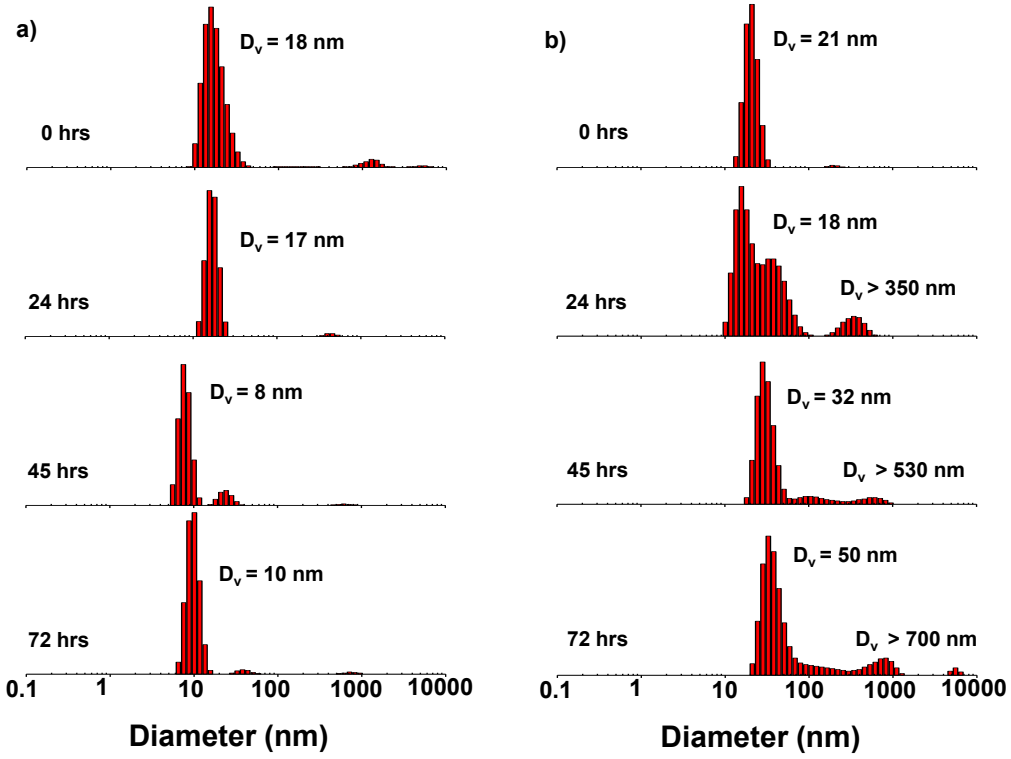

Figure 4.8. DLS diagram of aqueous ssABP-2-based micelles in the presence of 10 mM DTT (a) and 10 mM GSH (b) over time.

4.3.4 Loading and thiol-triggered drug release from Dox-loaded ssABP

Dox, a DNA intercalating anticancer drug in chemotherapy, was encapsulated in ssABP-2 micelles using a dialysis method. After intensive dialysis in deionized water, the prepared Dox-loaded micelles had a concentration of 2.4 mg/mL. Using the absorbance at λ_{max} = 497 nm (Figure B.2) and the pre-determined extinction coefficient, ε = 12,400 $M^{-1}cm^{-1}$ in a mixture of DMF/water = 5/1 v/v,[53] the loading level of Dox was determined to be 2.1%.

In response to reduction reactions, Dox can be released from Dox-loaded micelles and diffuse through the dialysis tubing to the outer water. Therefore, to study the thiol-triggered Dox release for the ssABP-2 system, aliquots of Dox-loaded ssABP-2 were dialyzed in the presence and absence of 10 mM GSH and the fluorescence increase of Dox in the outer water was monitored over time. Here, the reductive release of encapsulated Dox from micelles was examined using fluorescence spectroscopy. In order to eliminate concerns about the enhanced degradation of PLA in acidic pH, the pH of the outer was adjusted to pH = 7.4 using PBS solution for both control and 10 mM GSH aqueous solution. Figure B.3 shows the evolution of fluorescence spectra of outer water (λ_{ex} = 470 nm) over time. Using fluorescence intensities at λ_{max} = 590 nm, %Dox release over time was constructed in Figure 4.9. In the absence and presence of GSH, the gradual Dox release was followed for up to 46 hrs. Compared to the absence of GSH as a control, Dox release was enhanced to some degree in the presence of 10 mM GSH, as a consequence of the destabilization of Dox-loaded micelles upon the cleavage of disulfide linkages in response to GSH.

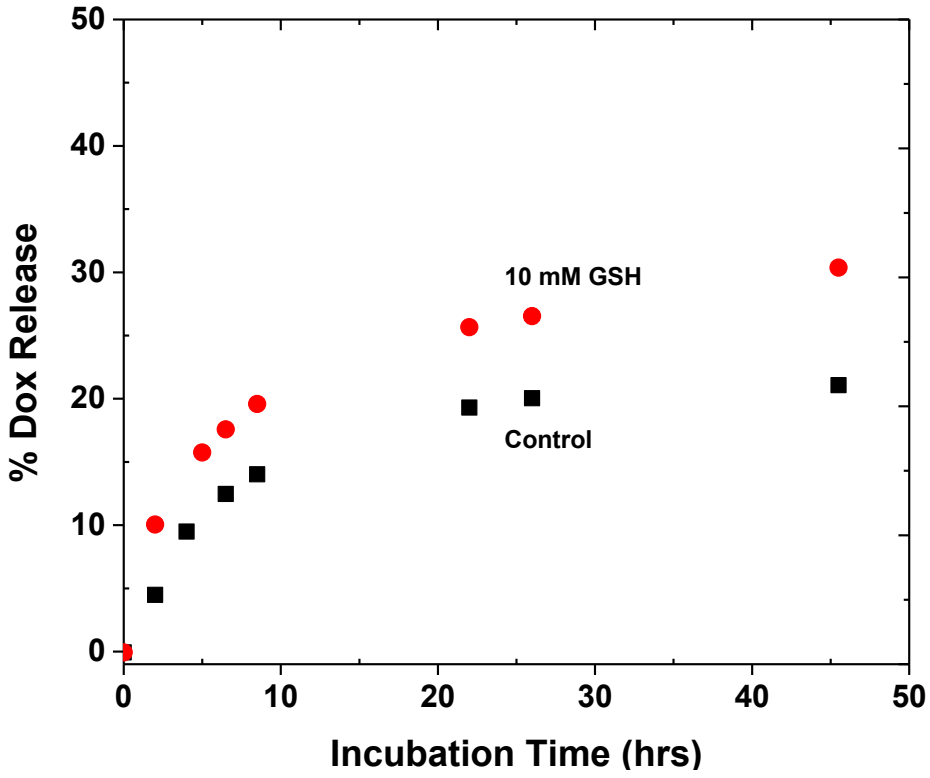

Figure 4.9. % Release profiles of Dox from Dox-loaded micelles in the absence (control) and presence of 10 mM GSH in PBS solution adjusted at pH = 7.4.

4.3.5 Non-specific protein interaction of ssABP-2 in vitro

Human serum albumin is one of the most abundant protein in blood serum and is found at concentrations ranging from 35-50 g/L. Here, ssABP micellar dispersion was incubated with different amounts of bovine serum albumin (BSA) at the weight ratio of micelles/BSA = 1/1 (13 g/L) and 1/2 (26 g/L) in PBS solution at pH = 7.4 (mimic of physiological conditions). Figure 4.10 shows the DLS diagrams of the mixtures after 90 hrs. For the mixtures at micelles/BSA = 1/1 w/w, a bimodal distribution appeared; each population appeared to be identical to ssABP-2 micelles and BSA in PBS solution. Furthermore, no occurrence of significant aggregation is observed. Similar results are found for the

mixture at micelles/BSA = 1/2 w/w. These results suggest that the presence of the hydrophilic PEO coronas provide enhanced colloidal stability to the nanoparticles in the presence of proteins during blood circulation and prevents from protein adsorption in physiological conditions.

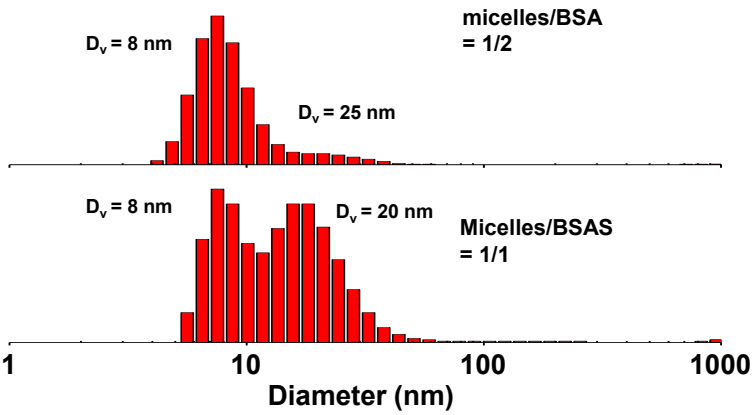

Figure 4.10. DLS diagrams of mixture consisting of ssABP-2 micelles and BSA at weight ratio of micelle/BSA = 1/1 (13 mg/mL) and 1/2 (26 mg/mL) in PBS solution at pH = 7.4 after 90 hrs.

4.4 Conclusion

New reduction-responsive triblock copolymers (ssABP-2) consisting of hydrophobic PLA and hydrophilic PEO blocks were synthesized by a combination of ROP and a facile carbodiimide coupling reaction. At concentrations above the CMC (13 μg/mL), aqueous self-assembled micelles with a diameter of 20 nm degraded to smaller nanostructures with diameter <10 nm in the presence of DTT, but to larger aggregates in the presence of GSH. Such changes in diameter are the consequence of reductive cleavage of disulfide linkages positioned in the middle of the ssABP-2 and forms smaller ABPs (PEO-b-PLA-SH or PEO-b-PLA-SS-GSH). The reductive-cleavage resulted in the destabilization of micelles, leading to the enhanced release of encapsulated

anticancer drugs. For biological perspectives, the ssABP micelles abstain from non-specific interaction with BSA proteins up to >90 hrs. These results suggest that ssABP and its self-assembled micelles could find their applications as reduction-responsive controlled/enhanced drug delivery nanocarriers. Moreover, these results show the successful synthetic design for the preparation of PLA-based monocleavable triblock copolymers with PEO as hydrophilic block, thereby expanding the possible combinations of hydrophobic and hydrophilic blocks that may be linked together in the construction of ABPs.

Chapter 5

Conclusion and future work

On the brink of bridging the gap between polymer research and pharmaceutical applications as drug delivery carriers, certain missing links awaits elucidation. A successful polymer-based drug delivery strategy relies on the use of biocompatible material, high encapsulation efficiency, long circulation time, and spatio-temporal drug release. With regards to drug release, one approach which holds great promise is the SRD platform. In particular, disulfide-thiol chemistry proposes a direct method for the controlled/enhanced release of encapsulated anticancer therapeutics in specific cells through the exploitation of the endogenous redox gradients. Further, careful incorporation of the disulfide linkages in the synthesis of well-defined block copolymers allowed for the investigation of morphological variance vs. stimuli-responsive drug release. The monocleavable system with the cleavable linkage in the middle of the central block of triblock copolymer was examined. Although often overlooked, a major aspect in the preparation of pharmaceutically exploitable ABP-based drug delivery systems is the ease of synthesis and the synthetic reproducibility. Furthermore, to expand on the possible combinations of polymers in the preparation of amphiphilic block copolymers different synthetic strategies were designed which rely on the incorporation of hydrophobic and biocompatible PLA with different hydrophilic blocks in a triblock copolymer system. In this thesis, two different methods for the preparation of PLA-based monocleavable triblock ABPs are proposed and the propensity of these systems towards drug delivery applications is presented.

To begin with, well-defined and reduction-responsive ss(PLA-b-POEOMA)$_2$ triblock copolymers were synthesized by a combination of ROP and ATRP. GPC and NMR results suggest that both polymerizations proceeded in a living manner allowing for the synthesis of well-defined ss(PLA-OH)$_2$ and ssABP-1 with monomodal and narrow molecular weight distribution with $M_w/M_n < 1.15$. Aqueous micellization of these ssABP-1 formed self-assembled micellar aggregates with disulfide-containing PLA cores. Because of the presence of central disulfides, these polymers degraded in response to thiols upon the cleavage of the disulfide linkage. Moreover, the presence of the hydrophobic core enabled the encapsulation of Dox as a model hydrophobic therapeutic drug. Results show that the thiol-triggered degradation resulted in enhanced release of encapsulated anticancer drug.

In the second strategy, ss(PLA-b-PEO)$_2$ were obtained through a combination of ROP and a facile coupling method. In this method, PEO was used as the hydrophilic block due to its promising properties in drug delivery applications; a great deal of research has shown the link between the presence of PEO as hydrophilic corona and the increase in circulation time as well as the reduction of non-specific protein interaction. Moreover, this line of work was directed towards discovering a synthetic method enabling the preparation of PLA-based block copolymers with PEO as the hydrophilic block. GPC and ^{1}H-NMR results suggest the synthesis of well-defined ssABP with narrow molecular weight distribution. These ssABP enabled the preparation of micellar nanoparticles where at concentrations above the CMC, 13 μg/mL, self-assembled micelles with a diameter of 20 nm are obtained. Due to the presence of thiol-responsive disulfide bonds in the core of the micelles, these nanoparticles responded to thiol-reducing agents such as GSH and DTT and underwent morphological changes. Indeed, these micelles degraded to smaller nanostructures with diameter <10 nm in the

presence of DTT, but to larger aggregates in the presence of GSH. Such changes in diameter are the consequence of reductive cleavage of disulfide linkages positioned in the middle of ssABP-2 and forms smaller ABPs (PEO-b-PLA-SH or PEO-b-PLA-SS-GSH). In addition, the reductive-cleavage resulted in the destabilization of micelles, leading to the enhanced release of encapsulated anticancer drugs. For biological perspectives, the ssABP-2 micelles did not exhibit non-specific interaction with BSA proteins for up to >90 hrs.

In summary, the present thesis examined different synthetic methods for the preparation of monocleavable triblock copolymer micelles with the thiol-reducing disulfide bond in the middle of the triblock copolymer. Although this system presented a certain potential towards drug delivery applications, certain improvements are needed. First of all, the monocleavable system exhibits reduction-responsive drug release to some degree. One potential solution to improve drug release could be the incorporation of multiple disulfide groups into the polymer to further disrupt the HS-ABP micelles generated and ensure complete drug release. This multicleavable system (shown in Figure 1.4c) demonstrates rapid drug release through main-chain cleavage mechanism.[35a] However, complexity in the design of PLA-related systems can pose a problem. Moreover, as mentioned earlier, there exist other parameters that need to be tuned for a successful drug delivery system to see the light of day. One prominent example is the increase in circulation time for the nanoparticles traveling throughout the bloodstream. Indeed, these nanoparticles escape the blood circulation and enter cancer tissues through the Enhanced-Permeation and Retention (EPR) effect. However, to fully exploit this mechanism and increase the uptake in cancer tissues these nanoparticles need to remain in circulation long enough to encounter the tumor tissues. A lot of research has shown that PEO as hydrophilic block increases residence time while reducing non-specific protein

interaction; however more work is needed to determine the exact mechanism of this phenomenon for its full exploitation. Finally, a thorough understanding of the interaction between the drug and the core forming block is necessary to increase drug encapsulation and reduce premature drug release, both important parameters governing the pharmacokinetics of the drug delivery system. For example, the glass-transition temperature (T_g) of the polymer constituting the core can have an impact on the loading and release profile of the encapsulated drug. A polymer with a high T_g will be characterized by a crystalline state thereby reducing the interactions between the nanocarrier core and the drug, as well as creating a network impeding drug diffusion; ultimately, reducing both drug loading and release. Therefore, strategies to reduce the T_g of the PLA core are greatly needed.

References

[1] J. W. Nichols, Y. H. Bae, *Nano Today* **2012**, *7*, 606-618.

[2] aY. H. Bae, K. Park, *Journal of Controlled Release* **2011**, *153*, 198-205; bO. C. Farokhzad, R. Langer, *ACS Nano* **2009**, *3*, 16–20.

[3] N. Nishiyama, K. Kataoka, *Advances in Polymer Science* **2006**, *193*, 67-101.

[4] K. Strebhardt, A. Ullrich, *Nature Reviews Cancer* **2008**, *8*, 473-480.

[5] L. Zhang, Y. Li, J. C. Yu, *Journal of Materials Chemistry B* **2014**, *2*, 452.

[6] aS. Majumdar, T. J. Siahaan, *Medicinal research reviews* **2012**, *32*, 637-658; bA. G. Cheetham, Y. C. Ou, P. Zhang, H. Cui, *Chemical communications* **2014**, *50*, 6039-6042; cM. Lelle, S. U. Frick, K. Steinbrink, K. Peneva, *Journal of Peptide Science* **2014**, *20*, 323–333.

[7] aS. Zalipsky, *Bioconjugate Chemistry* **1995**, *6*, 150-165; bJ. Khandare, T. Minko, *Progress in Polymer Science* **2006**, *31*, 359-397.

[8] A. Blanazs, S. P. Armes, A. J. Ryan, *Macromol Rapid Communications* **2009**, *30*, 267-277.

[9] K. E. Uhrich, S. M. Cannizzaro, R. S. Langer, K. M. Shakesheff, *Chemical Reviews* **1999**, *99*, 3181-3198.

[10] C. Li, S. Wallace, *Advanced drug delivery reviews* **2008**, *60*, 886-898.

[11] aE. Gillies, J. Frechet, *Drug Discovery Today* **2005**, *10*, 35-43; bM. Liu, J. M. J. Fréchet, *Pharmaceutical Science & Technology Today* **1999**, *2*, 393-401.

[12] aT. R. Hoare, D. S. Kohane, *Polymer* **2008**, *49*, 1993-2007; bA. S. Hoffman, *Advanced drug delivery reviews* **2012**, *64*, 18-23.

[13] K. Letchford, H. Burt, *European Journal of Pharmaceutics and Biopharmaceutics* **2007**, *65*, 259-269.

[14] aM. Moffitt, K. Khougaz, A. Eisenberg, *Accounts of Chemical Research* **1996**, *29*, 95-102; bG. Riess, *Progress in Polymer Science* **2003**, *28*, 1107-1170.

[15] C. Allen, D. Maysinger, A. Eisenberg, *Colloids and Surfaces B: Biointerfaces* **1999**, *16*, 3-27.

[16] J. Rodriguezhernandez, F. Checot, Y. Gnanou, S. Lecommandoux, *Progress in Polymer Science* **2005**, *30*, 691-724.

[17] aH. Hillaireau, P. Couvreur, *Cellular and Molecular Life Sciences* **2009**, *66*, 2873-2896; bA. S. Mikhail, C. Allen, *Journal of Controlled Release* **2009**, *138*, 214-223; cS. M. Moghimi, A. C. Hunter, J. C. Murray, *Pharmacological Reviews* **2001**, *53*, 283–318.

[18] aR. K. Jain, *Advanced drug delivery reviews* **2001**, *46*, 149–168; bS. k. Hobbs, W. L. Monsky, F. Yuan, G. W. Roberts, L. Griffith, V. P. Torchilin, R. K. Jain, *Proceedings of the National Academy of Sciences* **1998**, *95*, 4607–4612.

[19] K. Iwai, H. Maeda, T. Konno, *Cancer Research* **1984**, *44*, 2115-2121.

[20] Y. Matsumura, H. Maeda, *Cancer Research* **1986**, *46*, 6387-6392.

[21] K. Raemdonck, K. Braeckmans, J. Demeester, S. C. De Smedt, *Chemical Society reviews* **2014**, *43*, 444-472.
[22] Y. Zhang, H. F. Chan, K. W. Leong, *Advanced drug delivery reviews* **2013**, *65*, 104-120.
[23] C. Vauthier, K. Bouchemal, *Pharmaceutical research* **2009**, *26*, 1025-1058.
[24] Z. Zhang, D. W. Grijpma, J. Feijen, *Journal of Controlled Release* **2006**, *111*, 263-270.
[25] Q. Zhang, N. R. Ko, J. K. Oh, *Chemical communications* **2012**, *48*, 7542-7552.
[26] aV. Bulmus, Y. Chan, Q. Nguyen, H. L. Tran, *Macromolecular bioscience* **2007**, *7*, 446-455; bN. Murthy, M. Xu, S. Schuck, J. Kunisawa, N. Shastri, J. M. Frechet, *Proceedings of the National Academy of Sciences* **2003**, *100*, 4995-5000.
[27] aS. Kumar, J.-F. Allard, D. Morris, Y. L. Dory, M. Lepage, Y. Zhao, *Journal of Materials Chemistry* **2012**, *22*, 7252; bA. P. Goodwin, J. L. Mynar, Y. Ma, G. R. Fleming, J. M. J. Frechet, *Journal of the American Chemical Society* **2005**, *127*, 9952-9953; cH. Zhao, E. S. Sterner, E. B. Coughlin, P. Theato, *Macromolecules* **2012**, *45*, 1723-1736.
[28] Y. Wang, H. Xu, X. Zhang, *Advanced Materials* **2009**, *21*, 2849-2864.
[29] P. A. Fernandes, M. J. Ramos, *Chemistry European Journal* **2004**, *10*, 257-266.
[30] aJ. M. Estrela, A. Ortega, E. Obrador, *Critical reviews in clinical laboratory sciences* **2006**, *43*, 143-181; bG. Saito, J. A. Swanson, K.-D. Lee, *Advanced drug delivery reviews* **2003**, *55*, 199–215.
[31] aN. Traverso, R. Ricciarelli, M. Nitti, B. Marengo, A. L. Furfaro, M. A. Pronzato, U. M. Marinari, C. Domenicotti, *Oxidative medicine and cellular longevity* **2013**, *2013*, 972913; bA. Russo, W. DeGraff, N. Friedman, J. B. Mitchell, *Cancer Research* **1986**, *46*, 2845-2848; cD. S. Manickam, J. Li, D. A. Putt, Q. H. Zhou, C. Wu, L. H. Lash, D. Oupicky, *Journal of Controlled Release* **2010**, *141*, 77-84.
[32] C. J. Rijcken, O. Soga, W. E. Hennink, C. F. van Nostrum, *Journal of Controlled Release* **2007**, *120*, 131-148.
[33] aL.-Y. Tang, Y.-C. Wang, Y. Li, J.-Z. Du, J. Wang, *Bioconjugate Chemistry* **2009**, *20*, 1095–1099; bB. Khorsand, A. Cunningham, Q. Zhang, K. Oh Jung, *Biomacromolecules* **2011**, *12*, 3819-3825; cJ. Liu, Y. Pang, W. Huang, X. Huang, L. Meng, X. Zhu, Y. Zhou, D. Yan, *Biomacromolecules* **2011**, *12*, 1567-1577; dL.-Y. Tang, Y.-C. Wang, Y. Li, J.-Z. Du, J. Wang, *Bioconjugate Chemistry* **2009**, *20*, 1095-1099; eA. Klaikherd, C. Nagamani, S. Thayumanavan, *Journal of the American Chemical Society* **2009**, *131*, 4830–4838; fH.-Y. Wen, H.-Q. Dong, W.-j. Xie, Y.-Y. Li, K. Wang, G. M. Pauletti, D.-L. Shi, *Chemical communications* **2011**, *47*, 3550-3552; gH. Sun, B. Guo, X. Li, R. Cheng, F. Meng, H. Liu, Z. Zhong, *Biomacromolecules* **2010**, *11*, 848-854; hW. Yuan, H. Zou, W. Guo, T. Shen, J. Ren, *Polymer Chemistry* **2013**, *4*, 2658-2661; iW. Chen, Y. Zou, F. Meng, R. Cheng, C. Deng, J. Feijen, Z. Zhong, *Biomacromolecules* **2014**, *15*, 900-907; jJ. Xuan, D. Han, H. Xia, Y. Zhao, *Langmuir* **2014**, *30*, 410-417.

[34] aQ. Zhang, S. Aleksanian, S. M. Noh, J. K. Oh, *Polymer Chemistry* **2013**, *4*, 351-359; bJ. Dai, S. Lin, D. Cheng, S. Zou, X. Shuai, *Angewandte Chemie International Edition* **2011**, *50*, 9404-9408; cL. Yuan, J. Liu, J. Wen, H. Zhao, *Langmuir* **2012**, *28*, 11232-11240; dJ.-H. Ryu, R. Roy, J. Ventura, S. Thayumanavan, *Langmuir* **2010**, *26*, 7086-7092; eB. Khorsand, G. Lapointe, C. Brett, J. K. Oh, *Biomacromolecules* **2013**, *14*, 2103-2111.

[35] aA. Nelson-Mendez, S. Aleksanian, M. Oh, H.-S. Lim, J. K. Oh, *Soft Matter* **2011**, *7*, 7441-7452; bD. Han, X. Tong, Y. Zhao, *Langmuir* **2012**, *28*, 2327-2331; cJ. Liu, Y. Pang, W. Huang, Z. Zhu, X. Zhu, Y. Zhou, D. Yan, *Biomacromolecules* **2011**, *12*, 2407-2415; dS. Aleksanian, B. Khorsand, R. Schmidt, J. K. Oh, *Polymer Chemistry* **2012**, *3*, 2138; eH. Fan, J. Huang, Y. Li, J. Yu, J. Chen, *Polymer* **2010**, *51*, 5107-5114; fR. Tong, H. Xia, X. Lu, *Journal of Material Chemistry B* **2013**, *1*, 886-894.

[36] aB. Khorsand, R. Schmidt, J. K. Oh, *Macromolecular Rapid Communications* **2011**, *32*, 1652-1657; bA. Cunningham, J. K. Oh, *Macromolecular Rapid Communications* **2013**, *34*, 163-168.

[37] L. Sun, W. Liu, C. M. Dong, *Chemical communications* **2011**, *47*, 11282-11284.

[38] D. L. Liu, X. Chang, C. M. Dong, *Chemical communications* **2013**, *49*, 1229-1231.

[39] aX. Jiang, M. Zhang, S. Li, W. Shao, Y. Zhao, *Chemical communications* **2012**, *48*, 9906-9908; bS. Li, C. Ye, G. Zhao, M. Zhang, Y. Zhao, *Journal of Polymer Science Part A: Polymer Chemistry* **2012**, *50*, 3135-3148; cM. Zhang, H. Liu, W. Shao, K. Miao, Y. Zhao, *Macromolecules* **2013**, *46*, 1325-1336.

[40] Q. Zhang, S. Aleksanian, A. Cunningham, J. K. Oh, *ACS Symposium Series Volume 1101. Progress in Controlled Radical Polymerization. Eds: K. Matyjaszewski, B. S. Sumerlin, and N. V. Tsarevsky* **2013**, *Chapter 19*, 289-302.

[41] S. Penczek, M. Cypryk, A. Duda, P. Kubisa, S. Slomkowski, *Progress in Polymer Science* **2007**, *32*, 247-282.

[42] R. A. Jain, *Biomaterials* **2000**, *21*, 2475 - 2490.

[43] Suming Li , Aurelie Girard, Henri Garreau, M. Vert, *Polymer Degradation and Stability* **2001**, *71*, 61 - 67.

[44] L. S. Nair, C. T. Laurencin, *Progress in Polymer Science* **2007**, *32*, 762-798.

[45] aG. Gaucher, R. H. Marchessault, J. C. Leroux, *Journal of Controlled Release* **2010**, *143*, 2-12; bZ. Cao, Q. Yu, H. Xue, G. Cheng, S. Jiang, *Angewandte Chemie International Edition* **2010**, *49*, 3771-3776.

[46] aC. Hiemstra, W. Zhou, Z. Zhong, M. Wouters, J. Feijen, *Journal of the American Chemical Society* **2007**, *129*, 9918-9926; bQ. Wang, L. Wang, M. S. Detamore, C. Berkland, *Advanced Materials* **2008**, *20*, 236-239; cB. L. Dargaville, C. Vaquette, H. Peng, F. Rasoul, Y. Q. Chau, J. J. Cooper-White, J. H. Campbell, A. K. Whittaker, *Biomacromolecules* **2011**, *12*, 3856-3869.

[47] aF. Y. Cheng, C. H. Su, P. C. Wu, C. S. Yeh, *Chemical communications* **2010**, *46*, 3167-3169; bT. K. Jain, J. Richey, M. Strand, D. L. Leslie-Pelecky, C. A. Flask, V. Labhasetwar, *Biomaterials* **2008**, *29*, 4012-4021; cJ. Yang, C. H. Lee, H. J. Ko, J. S.

Suh, H. G. Yoon, K. Lee, Y. M. Huh, S. Haam, *Angewandte Chemie International Edition* **2007**, *46*, 8836-8839.
[48] J. K. Oh, *Soft Matter* **2011**, *7*, 5096.
[49] aA. van der Ende, T. Croce, S. Hamilton, V. Sathiyakumar, E. Harth, *Soft Matter* **2009**, *5*, 1417; bQ. Chen, S. Liang, G. A. Thouas, *Soft Matter* **2011**, *7*, 6484; cN. Rapoport, *Progress in Polymer Science* **2007**, *32*, 962-990.
[50] Y. Liu, A. H. Ghassemi, W. E. Hennink, S. P. Schwendeman, *Biomaterials* **2012**, *33*, 7584-7593.
[51] H.-F. Liang, S.-C. Chen, M.-C. Chen, P.-W. Lee, C.-T. Chen, H.-W. Sung, *Bioconjugate Chemistry* **2006**, *17*, 291 − 299.
[52] aN. R. Ko, K. Yao, C. Tang, J. K. Oh, *Journal of Polymer Science Part A: Polymer Chemistry* **2013**, *51*, 3071-3080; bN. R. Ko, G. Sabbatier, A. Cunningham, G. Laroche, J. K. Oh, *Macromolecular Rapid Communications* **2014**, *35*, 447-453.
[53] N. Chan, S. Y. An, J. K. Oh, *Polymer Chemistry* **2014**, *5*, 1637-1649.
[54] A. P. Gupta, V. Kumar, *European Polymer Journal* **2007**, *43*, 4053-4074.
[55] O. Dechy-Cabaret, B. Martin-Vaca, D. Bourissou, *Chemical Reviews* **2004**, *104*, 6147−6176.
[56] aH. R. Kricheldorfl, I. Kreiser-Saunders, *Die Makromolekulare Chemie* **1990**, *191*, 1057-1066; bH. R. Kricheldorfl, *Chemosphere* **2001**, *43*, 49 - 54.
[57] aA. Kowalski, A. Duda, S. Penczek, *Macromolecular Rapid Communications* **1998**, *19*, 567-572; bH. R. Kricheldorf, I. Kreiser-Saunders, C. Boettcher, *Polymer* **1995**, *36*, 1253-1259; cH. R. Kricheldorf, I. Kreiser-Saunders, A. Stricker, *Macromolecules* **2000**, *33*, 702-709.
[58] M. Kato, M. Kamigaito, M. Sawamoto, T. Higashimura, *Macromolecules* **1995**, *28*, 1721-1723.
[59] J.-S. Wang, K. Matyjaszewski, *Journal of the American Chemical Society* **1995**, *117*, 5614-5615.
[60] T. E. Patten, K. Matyjaszewski, *Advanced Materials* **1998**, *10*, 901-915.
[61] aD. A. Singleton, D. T. N. III, N. Jahed, K. Matyjaszewski, *Macromolecules* **2003**, *36*, 8609-8616; bK. Matyjaszewski, *Macromolecular Symposia* **1998**, *134*, 105-118; cD. Konkolewicz, Y. Wang, P. Krys, M. Zhong, A. A. Isse, A. Gennaro, K. Matyjaszewski, *Polymer Chemistry* **2014**, *5*, 4409; dD. Konkolewicz, Y. Wang, M. Zhong, P. Krys, A. A. Isse, A. Gennaro, K. Matyjaszewski, *Macromolecules* **2013**, *46*, 8749-8772.
[62] J. Xia, K. Matyjaszewski, *Chemical Reviews* **2001**, *101*, 2921−2990.
[63] Schott-Geräte, **http://www.mtpgroup.nl/amm-laboratory-course.aspx accessed on July 2014**.
[64] J. Eastoe, J. S. Dalton, *Advances in Colloid and Interface Science* **2000**, *85*, 103 - 144.
[65] P. Greenspan, S. D. Fowler, *Journal of Lipid Research* **1985**, *26*, 781-789.
[66] I. Astafieva, X. F. Zhong, A. Eisenberg, *Macromolecules* **1993**, *26*, 7339-7352.
[67] N. Sarkar, K. Das, D. N. Nath, K. Bhattacharyya, *Langmuir* **1994**, *10*, 326-329.

[68] M. C. A. Stuart, J. C. van de Pas, J. B. F. N. Engberts, *Journal of Physical Organic Chemistry* **2005**, *18*, 929-934.
[69] D. H. Yu, Q. Lu, J. Xie, C. Fang, H. Z. Chen, *Biomaterials* **2010**, *31*, 2278-2292.
[70] X. L. Wu, J. H. Kim, H. Koo, S. M. Bae, H. Shin, M. S. Kim, B.-H. Lee, R.-W. Park, I.-S. Kim, K. Choi, I. C. Kwon, K. Kim, D. S. Lee, *Bioconjugate Chemistry* **2010**, *21*, 208-213.
[71] K. Loomis, K. McNeeley, R. V. Bellamkonda, *Soft Matter* **2011**, *7*, 839.
[72] aA. Ghosh, M. Haverick, K. Stump, X. Yang, M. F. Tweedle, J. E. Goldberger, *Journal of the American Chemical Society* **2012**, *134*, 3647-3650; bT. H. Ku, M. P. Chien, M. P. Thompson, R. S. Sinkovits, N. H. Olson, T. S. Baker, N. C. Gianneschi, *Journal of the American Chemical Society* **2011**, *133*, 8392-8395.
[73] aR. Cheng, F. Feng, F. Meng, C. Deng, J. Feijen, Z. Zhong, *Journal of Controlled Release* **2011**, *152*, 2-12; bF. Meng, W. E. Hennink, Z. Zhong, *Biomaterials* **2009**, *30*, 2180-2198.
[74] J. Jiang, X. Tong, D. Morris, Y. Zhao, *Macromolecules* **2006**, *39*, 4633-4640.
[75] aJ. Chen, C. Wu, D. Oupicky, *Biomacromolecules* **2009**, *10*, 2921–2927; bP. Pinnel, A. Mendez-Nelson, S. M. Noh, J. H. Nam, J. K. Oh, *Macromolecular Chemistry and Physics* **2012**, *213*, 678-685.
[76] M. H. Lee, Z. Yang, C. W. Lim, Y. H. Lee, D. Sun, C. Kang, J. S. Kim, *Chemical Reviews* **2013**, *113*, 5071-5109.
[77] aD. J. Phillips, M. I. Gibson, *Chemical communications* **2012**, *48*, 1054-1056; bQ. Zhang, S. M. Noh, J. H. Nam, H. W. Jung, J. M. Park, J. K. Oh, *Macromolecular Rapid Communications* **2012**, *33*, 1528-1534; cL.-J. Zhang, B.-T. Dong, F.-S. Du, Z.-C. Li, *Macromolecules* **2012**, *45*, 8580-8587; dK. Rahimian-Bajgiran, N. Chan, Q. Zhang, S. M. Noh, H. I. Lee, J. K. Oh, *Chemical communications* **2013**, *49*, 807-809.
[78] aM. Zhang, L. Yang, S. Yurt, M. J. Misner, J. T. Chen, E. B. Coughlin, D. Venkataraman, T. P. Russell, *Advanced Materials* **2007**, *19*, 1571-1576; bH. Zhao, W. Gu, E. Sterner, T. P. Russell, E. B. Coughlin, P. Theato, *Macromolecules* **2011**, *44*, 6433-6440.
[79] aN. R. Ko, G. Sabbatier, A. Cunningham, G. Laroche, J. K. Oh, *Macromolecular Rapid Communications* **2014**, *35*, 447-453; bH. Zhao, W. Gu, M. W. Thielke, E. Sterner, T. Tsai, T. P. Russell, E. B. Coughlin, P. Theato, *Macromolecules* **2013**, *46*, 5195-5201.
[80] J. K. Oh, R. Drumright, D. J. Siegwart, K. Matyjaszewski, *Progress in Polymer Science* **2008**, *33*, 448-477.
[81] aY. Zhao, *Macromolecules* **2012**, *45*, 3647-3657; bA. W. Jackson, D. A. Fulton, *Polymer Chemistry* **2013**, *4*, 31-45.
[82] aH. Wei, R.-X. Zhuo, X.-Z. Zhang, *Progress in Polymer Science* **2013**, *38*, 503-535; bM. Huo, J. Yuan, L. Tao, Y. Wei, *Polymer Chemistry* **2014**, *5*, 1519-1528.
[83] aA. P. Bapat, J. G. Ray, D. A. Savin, B. S. Sumerlin, *Macromolecules* **2013**, *46*, 2188-2198; bZ. Zhang, L. Yin, C. Tu, Z. Song, Y. Zhang, Y. Xu, R. Tong, Q. Zhou, J.

Ren, J. Cheng, *ACS Macro Letters* **2013**, *2*, 40-44; cW. Chen, M. Zheng, F. Meng, R. Cheng, C. Deng, J. Feijen, Z. Zhong, *Biomacromolecules* **2013**, *14*, 1214-1222; dR. Wei, L. Cheng, M. Zheng, R. Cheng, F. Meng, C. Deng, Z. Zhong, *Biomacromolecules* **2012**, *13*, 2429-2438; eZ. Jia, L. Wong, T. P. Davis, V. Bulmus, *Biomacromolecules* **2008**, *9*, 3106-3113; fJ.-H. Ryu, R. T. Chacko, S. Jiwpanich, S. Bickerton, R. P. Babu, S. Thayumanavan, *Journal of the American Chemical Society* **2010**, *132*, 17227-17235; gY.-L. Li, L. Zhu, Z. Liu, R. Cheng, F. Meng, J.-H. Cui, S.-J. Ji, Z. Zhong, *Angewandte Chemie International Edition* **2009**, *48*, 9914-9918, S9914/9911-S9914/9914.

[84] D. Han, X. Tong, Y. Zhao, *Langmuir* **2012**, *28*, 2327-2331.

[85] M. Ding, J. Li, X. He, N. Song, H. Tan, Y. Zhang, L. Zhou, Q. Gu, H. Deng, Q. Fu, *Advanced Materials* **2012**, *24*, 3639-3645, S3639/3631-S3639/3642.

[86] K. Knop, R. Hoogenboom, D. Fischer, U. S. Schubert, *Angewandte Chemie International Edition* **2010**, *49*, 6288-6308.

[87] O. C. Farokhzad, J. Cheng, B. A. Teply, I. Sherifi, S. Jon, P. W. Kantoff, J. P. Richie, R. Langer, *Proceedings of the National Academy of Sciences* **2006**, *103*, 6315-6320.

Appendix A

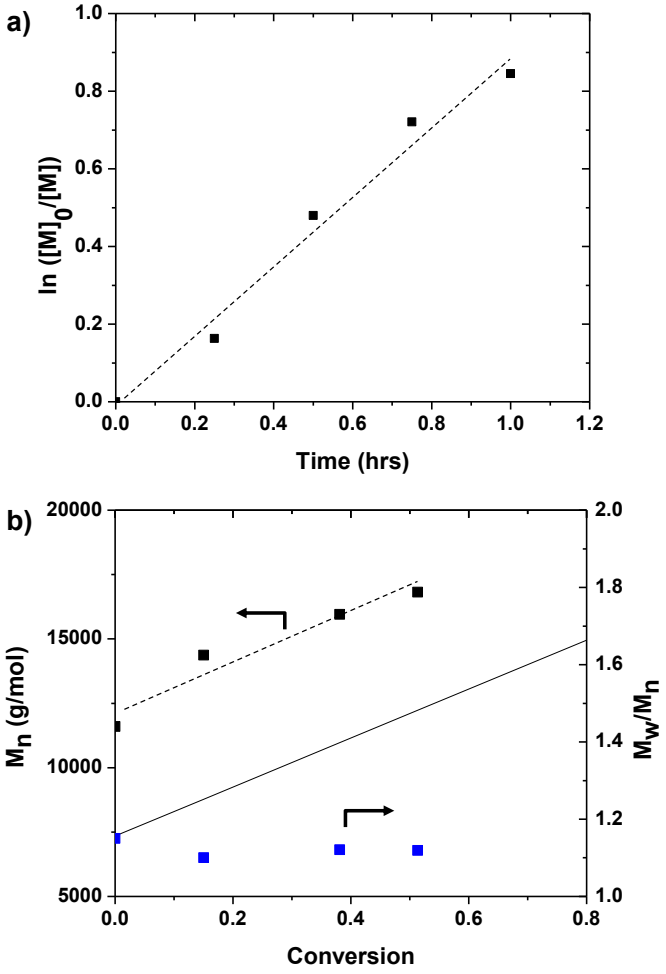

Figure A.1. First-order kinetic plot (a) and evolution of molecular weight and molecular weight distribution over conversion (b) for ATRP of OEOMA in the presence of ss(PLA-Br)$_2$ macroinitiator in THF at 47 °C. Conditions: [OEOMA]$_0$/[ss(PLA-Br)$_2$]$_0$/[CuBr/PMDETA]$_0$ = 20/1/0.5; OEOMA/THF = 0.8/1 wt/wt. The dotted lines are linear fits and the line in (b) is the theoretically predicted molecular weight over conversion.

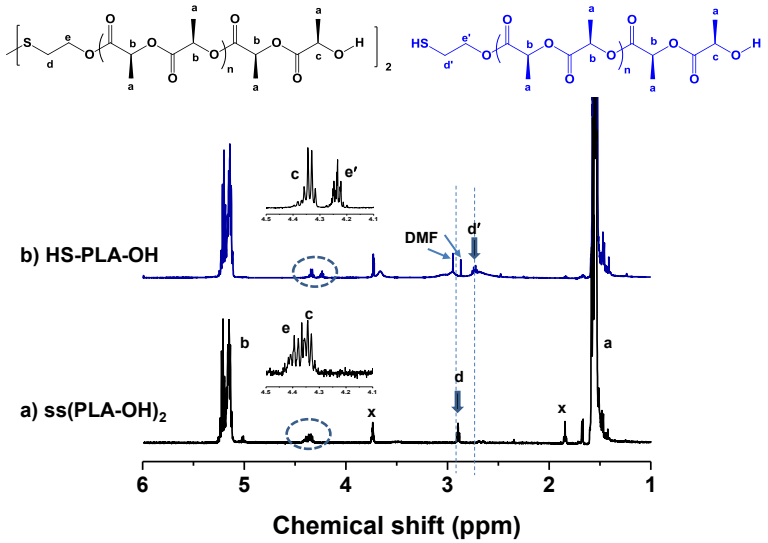

Figure A.2. ^{1}H-NMR spectra, in $CDCl_3$, of $ss(PLA\text{-}OH)_2$ (a) and DTT-mediated degraded product (HS-PLA-OH) (b) yielded by the cleavage of disulfides. X denotes a residure of THF.

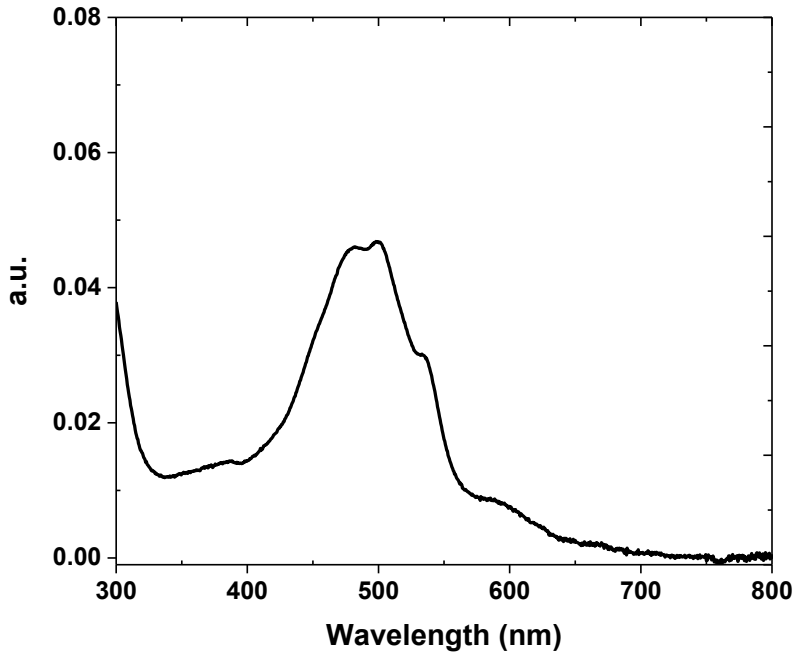

Figure A.3. UV/Vis spectrum of Dox-loaded micelles in a mixture of DMF/water = 5/1 v/v.

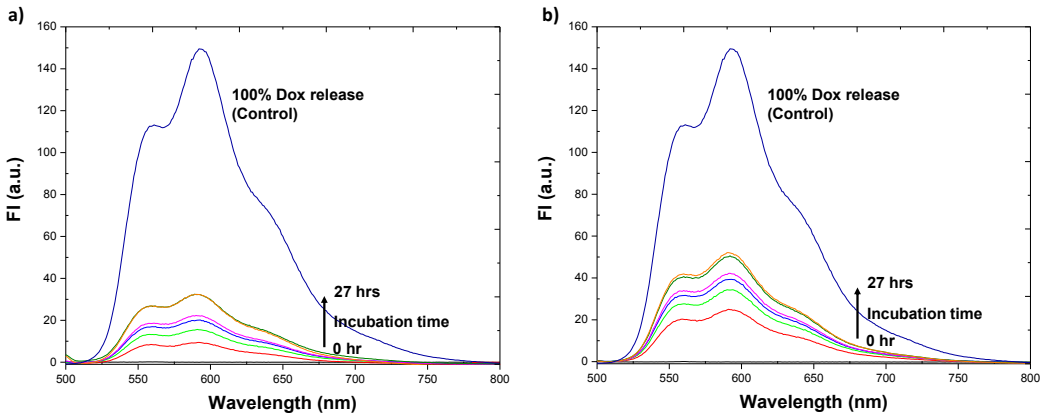

Figure A.4. Evolution of fluorescence spectra of outer water in the absence (a) and presence (b) of 10 mM GSH along with fluorescence spectra used for normalization as a mimic of 100% drug release.

Appendix B

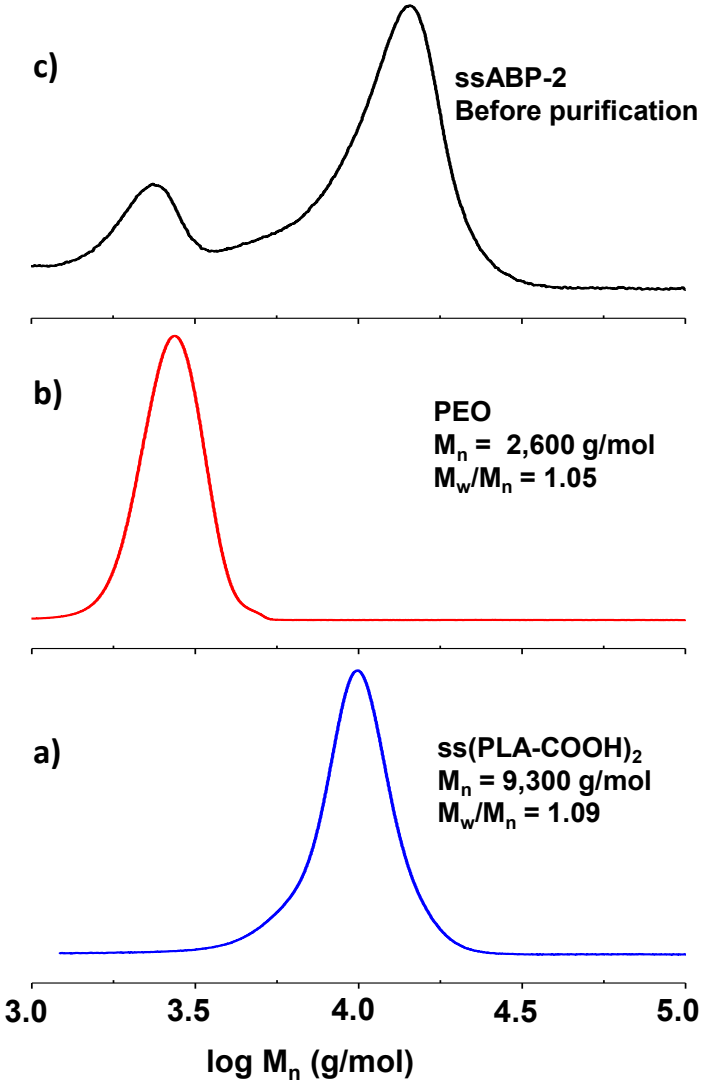

Figure B.1. GPC traces of ss(PLA-COOH)$_2$ (a), and PEO (b), and crude ssABP-2 before purification (c).

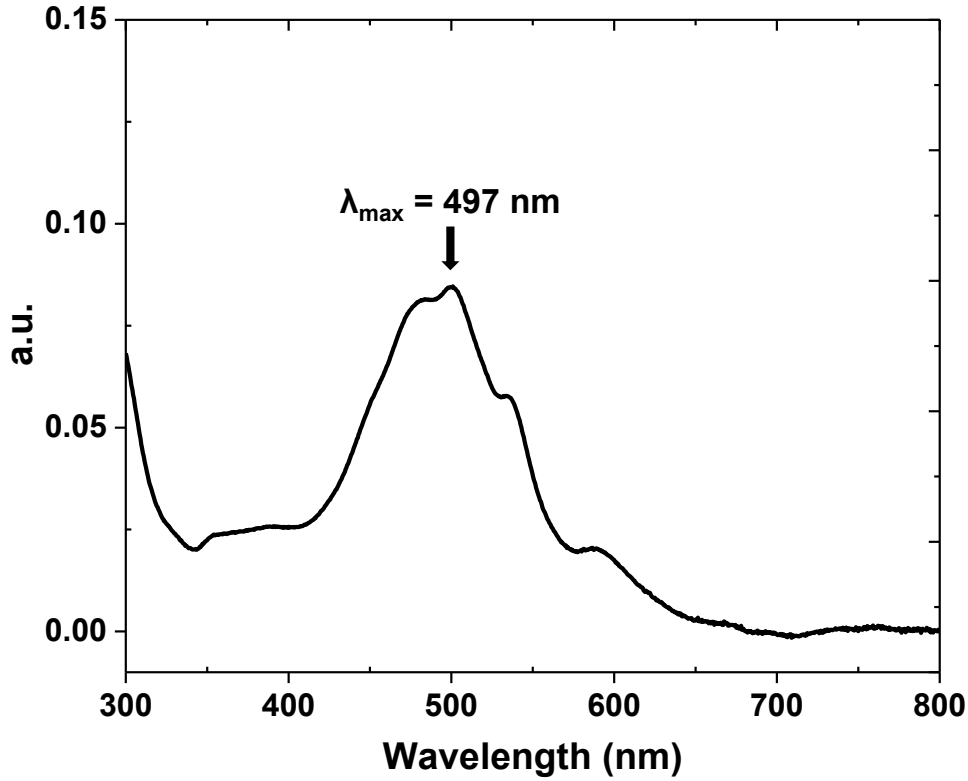

Figure B.2. UV/Vis spectrum of Dox-loaded micelles in a mixture of DMF/water = 5/1 v/v.

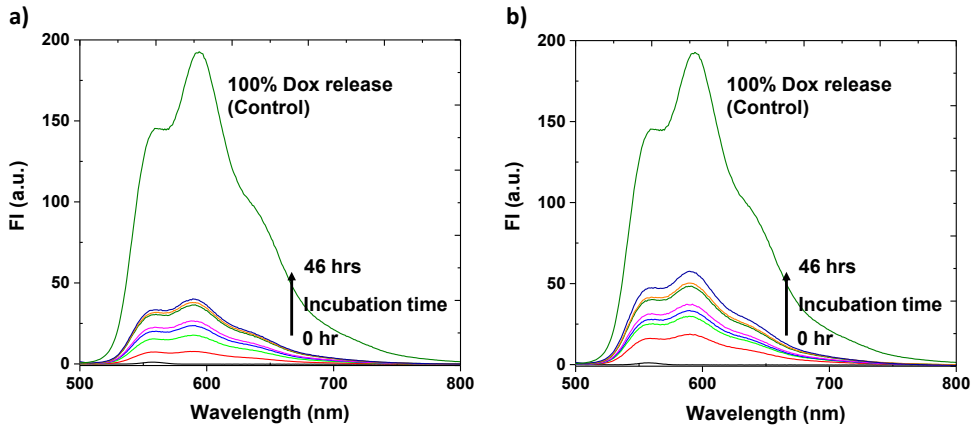

Figure B.3. Evolution of fluorescence spectra of outer water in the absence (a) and presence (b) of 10 mM GSH along with fluorescence spectra used for normalization as a mimic of 100% drug release.

Publications

A. Cunningham, N. R. Ko, J. K. Oh* Synthesis and reduction-responsive disassembly of PLA-based mono-cleavable micelles. *Colloids and surfaces B: Biointerfaces*, **2014**, In press, DOI: 10.1016/j.colsurfb.2014.08.002

N. R. Ko, G. Sabbatier, **A. Cunningham**, G. Laroche, J. K. Oh* Air-spun PLA fibers modified with reductively-sheddable hydrophilic surfaces for vascular tissue engineering: synthesis and surface modification. *Macromolecular Rapid Communications*, **2013**, 34, 163-168.

A. Cunningham, J. K. Oh* New design of thiol-responsive degradable polylactide-based block copolymer micelles. *Macromolecular Rapid Communications*, **2013**, 34, 163-168.

Q. Zhang, S. Aleksanian, **A. Cunningham**, J. K. Oh* New-Design of thiol-responsive degradable block copolymer micelles as controlled drug delivery vehicles. In *Progress in Controlled Radical Polymerization*; K. Matyjaszewski, B. S. Sumerlin, N. V. Tsarevsky. *ACS Symposium Series 1101*. American Chemical Society. Washington, DC, 2012. Chapter 19, pp 289-302.

B. K. Sourkohi, **A. Cunningham**, Q. Zhang, J. K. Oh* Biodegradable block copolymer micelles with thiol-responsive sheddable coronas. *Biomacromolecules*, **2011**, 12, 3819-3825.